A Study of the Difference in Process Zones at a Crack Tip and Incomplete Contact Edge

Zoë Clark

Lincoln College

University of Oxford

Thesis submitted for Degree of Masters of Science

September 2018

Acknowledgements:

David Hills, Robert Paynter, Jesús Vazquez Valeo and Rangarajan Ramesh.

Abstract

The aim of this research project was to compare the plastic stress fields in two, apparently very different, geometries and therefore find how they will behave in certain loading scenarios. The similarities in plastic zones in an incomplete contact edge problem under conditions of full stick or near full-stick, and a crack tip problem were analysed. In each case the normal load was held constant and the shear load applied in an oscillatory fashion. It is clear that in both cases there will be a stress concentration at the apex of the geometry of interest (i.e. the crack tip or contact edge) and this analysis will demonstrate how and why these differ. The contact problem has been analysed as if there is an infinite coefficient of friction and therefore no slip between plates, and it is shown why this is a valid simplification. The analysis started by using elasticity with violations of the yield condition and the Williams' solution, and then moved on to use computational analysis to calculate the steady state plastic zones. The output at the end of this project is a comparison between the steady state plastic region shapes and sizes when applying a constant symmetric load and oscillating antisymmetric load; we find that under these conditions the two different geometries give the same steady state stress field.

Table of Contents

1 Introduction/Motivation 5

2 Elastic Analysis: The Williams' Solution [] 7

2.1 Calculating the Stress Functions 8

2.2 Calculating the Stresses 11

2.2.1 Symmetric Terms 11

2.2.2 Antisymmetric Terms 13

2.2.3 Revised William's Solution 14

2.3 Calculating the Displacements 15

2.3.1 Symmetric Terms 16

2.3.2 Antisymmetric Terms 18

2.4 Size of the Yielded Region 19

2.4.1 Mode I 21

2.4.2 Mode II 23

3 Elastic Analysis: Giannakopoulos' Innovation [6] 26

4 Elastic Analysis: The No-Slip Edge Condition 29

5 Elastic Analysis: Mode Mixity in Contact Edge Geometry 31

6 Elastic Analysis: Results 34

6.1 Crack Tip 34

6.2 Incomplete Contact Interface 34

7 Plastic Analysis: Plastic Shakedown 36

8 Plastic Analysis: Defining the Variables 38

8.1 The Problem 38

8.2 Choosing Variables 39

8.2.1 Crack Tip 40

8.2.2 Contact Interface 41

8.3 Finding the Plastic Radii 42

8.3.1 Mode I 42

8.3.2 Mode II 44

9 Plastic Analysis: Simplifying Assumptions 51

9.1 Displacement vs Load Control 46

9.2 The Use of a Keyhole at the Crack Tip 46

9.3 Setting Displacements to zero rather than releasing them 47

10 Plastic Analysis: Creating the Finite Element Model 51

10.1 Creating the Geometry 48

10.2 Applying the Displacements 50

11 Plastic Analysis: Results from Finite Element Analysis 51

11.1 Comparison to Elasticity Model 51

11.2 Introducing Plasticity 52

11.3 Loading in One Direction 53

11.4 Positive and Negative Loading 56

11.5 Contact Edge 60

11.5.1 Attachment to an Example Problem 60

11.5.2 Modelling 63

11.6 Plastic Analysis: Verification of No Slip Edge Condition 67

12 Conclusions and Discussion 70

13 Further Work 71

1 *Introduction/Motivation*

There are fundamentally four different types of contact; incomplete when contact size increases with applied normal force; complete where contact area is fixed by one of the bodies and so doesn't change with normal force; receding where a larger normal force will decrease contact size and common edge where the contact area is fixed by both bodies.

The aim of this project is to investigate the similarities between the process zones of a crack tip and an incomplete contact edge. To do this analysis we must first consider the Williams' solution. The Williams' solution is commonly used in solid mechanics problems. The first section of this thesis will go into detail of how to use the Williams' solution to calculate the stresses and strains within a problem.

In solid mechanics problems which exceed the yield stress there are various different way to deal with the analysis. The simplest analysis can be done analytically and is based on 'elasticity and violations'. This means that a stress field is generated for a certain problem and it is then assumed that any area which violates the yield condition (i.e. is at a stress equal to or greater than the yield stress) is at the yield stress. By making the simplifying assumption that any stresses above the yield stress are equal to the yield stress we in turn violate the equilibrium conditions, and no re-distribution takes place. For a crack tip theory predicts that the plasticity zone will double due to the redistribution of stresses; for small scale yielding this is an acceptable as the error due to the yielded zone is still small. However as the yielded region gets larger this method breaks down and can be shown to not be very accurate.

Alternatively, we must deal with plasticity by an iterative, numerical approach, normally the finite element method, so that regions of stresses above the yield condition are modelled as flowing, correctly satisfying the flow rules, and loads are redistributed throughout the body. This will inevitably lead to a larger yield zone and typically a slightly different shape too, compared with an 'elasticity plus

violations' approach. This process needs to be done through computational, iterative analysis as it cannot be done purely analytically. I will be using Abaqus for my analysis in this project.

The underlying reason for this work is that, if it can be shown that an incomplete contact edge is like a crack suffering mode II loading, we can borrow all the result an experience of fracture mechanics under mode II loading and apply it to fretting fatigue problems, and this would help our understanding considerably.

In this thesis it is found that, due to the shakedown of stresses, the two situations become one and the same under an oscillatory shear load.

2 *Elastic Analysis: The Williams' Solution [1]*

In this thesis the Williams' solution is used in order to formulate the plasticity zones when we can assume the elasticity and violations approach is valid. This will only be valid if the plasticity zone is relatively small in relation to the total geometry being considered. After using this elasticity and violations approach the Williams solution will be further used to help set up the finite element model to look at what happens when we introduce plasticity.

The Williams' solution is a formulation to calculate the stresses near a sharp notch of included angle 2α within a 2D infinite sheet of material, when subjected to any remote loading conditions. It is commonly used to analyse a notch or a crack tip. We will also be applying it to an incomplete contact which is of similar geometry to a crack tip. The Williams' solution is formulated in terms of plane polar (r,θ) co-ordinates.

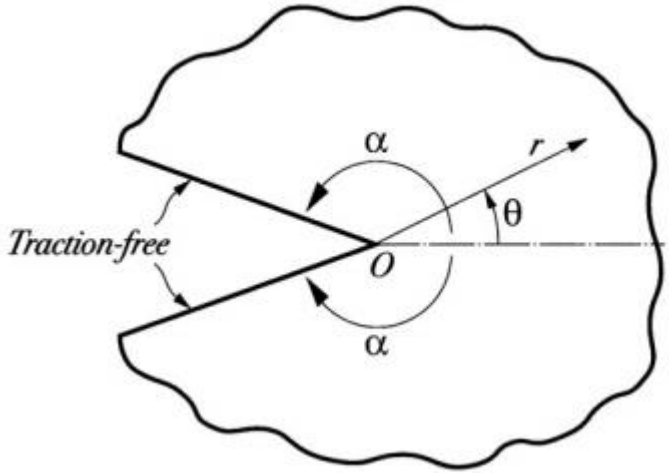


Figure 1 – The semi-infinite notch, from Barber's Book[2]

The Williams' solution may be applied to many different geometries to varying degrees of accuracy, however it will always be accurate when the distance (r) at which it is being examined is small compared to any other geometry. In simple terms, it will be accurate when one is looking close to the feature in relative terms.

2.1 Calculating the Stress Functions

The generalised Williams' solution is as follows. The first two, dominant, terms imply states of stress which vary with the square root of *r*; these are called the singular terms and go to infinity at a crack or notch tip. The square root singular terms are dominant at the crack tip/notch root as they have a negative exponent of r. Next, there are two terms called the T-stress terms which correspond to a lambda value of 1 and are therefore independent of radius. They are effectively just a constant term which is often ignored. The T-stress physically originates from remote loading parallel to the crack and, as such, it doesn't have a first order effect on fracture, giving

$$\sigma_{ij} = K_I r^{-1/2} f_I^{ij}(\theta) + K_{II} r^{-1/2} f_{II}^{ij}(\theta) + T_I g_I^{ij}(\theta) + T_{II} g_{II}^{ij}(\theta) + bounded\ terms \tag{1}$$

Then we have what are called the 'bounded terms'. These are terms which vary with *r* to an exponent of more than zero. These terms will obviously go to zero at the crack tip or notch and become infinite as *r* does.

Airy's stress functions are a common tool used in solid mechanics to describe the state of stress within a body. For the Williams' solution the following general Airy's stress function applies. It is important to note that this function includes contributions from both the symmetric (opening mode/mode *I*) and antisymmetric (shearing mode/mode *II*) terms.

$$\begin{aligned}\phi = r^{\lambda+1}\{&A_1 \cos((\lambda+1)\theta) \\ &+ A_2 \cos((\lambda-1)\theta) + A_3 \sin((\lambda+1)\theta) + A_4 \sin((\lambda-1)\theta)\}\end{aligned} \tag{2}$$

This stress function can be separated into the symmetric and antisymmetric parts. The symmetric terms, being the cosine terms as a cosine wave is even function, and the antisymmetric ones being the sine terms, might be written as follows

$$\phi_S = r^{\lambda+1}\{A_1 \cos((\lambda+1)\theta) + A_2 \cos((\lambda-1)\theta)\} \tag{3}$$

$$\Phi_A = r^{\lambda+1}\{A_3 \sin((\lambda+1)\theta) + A_4 \sin((\lambda-1)\theta)\} \quad (4)$$

Through the application of the Airy Stress Function we can calculate the stresses in polar co-ordinates the general solution can be found by imposing the traction free boundary conditions. A more involved calculation may be found in Barber (2) page 145.

At the free edges the following applies:

$$\theta = \pm\alpha, \quad \sigma_{\theta\theta} = \sigma_{r\theta} = 0\text{MPa} \quad (5)$$

In the symmetric case

$$\begin{bmatrix} (\lambda+1)\sin((\lambda+1)\alpha) & (\lambda-1)\sin((\lambda-1)\alpha) \\ (\lambda+1)\cos((\lambda+1)\alpha) & (\lambda+1)\cos((\lambda-1)\alpha) \end{bmatrix} \begin{Bmatrix} A_1 \\ A_2 \end{Bmatrix} = 0 \quad (6)$$

This matrix equation has three solutions, one of which is trivial (i.e. $A_1 = A_2 = A = 0$) and the other two are as follows.

$$\begin{Bmatrix} A_1 \\ A_2 \end{Bmatrix} = \begin{bmatrix} A(\lambda-1)\sin((\lambda-1)\alpha) \\ -A(\lambda+1)\sin((\lambda+1)\alpha) \end{bmatrix} \quad (7)$$

and

$$\begin{Bmatrix} A_1 \\ A_2 \end{Bmatrix} = \begin{bmatrix} A(\lambda+1)\cos((\lambda-1)\alpha) \\ -A(\lambda+1)\cos((\lambda+1)\alpha) \end{bmatrix} \quad (8)$$

In the antisymmetric case

$$\begin{bmatrix} (\lambda+1)\cos((\lambda+1)\alpha) & (\lambda-1)\cos((\lambda-1)\alpha) \\ (\lambda+1)\sin((\lambda+1)\alpha) & (\lambda+1)\sin((\lambda-1)\alpha) \end{bmatrix} \begin{Bmatrix} A_3 \\ A_4 \end{Bmatrix} = 0 \quad (9)$$

This matrix equation also has three solutions, one of which is trivial (i.e. $A_3 = A_4 = A = 0$) and the other two are as follows.

$$\begin{Bmatrix} A_3 \\ A_4 \end{Bmatrix} = \begin{bmatrix} A(\lambda-1)\cos((\lambda-1)\alpha) \\ -A(\lambda+1)cos((\lambda+1)\alpha) \end{bmatrix} \tag{10}$$

and

$$\begin{Bmatrix} A_3 \\ A_4 \end{Bmatrix} = \begin{bmatrix} A(\lambda+1)\sin((\lambda-1)\alpha) \\ -A(\lambda+1)sin((\lambda+1)\alpha) \end{bmatrix} \tag{11}$$

These solutions can then be substituted into the relevant Airy's Stress functions to give the following four equations.

$$\begin{aligned} \phi_{S1} = Ar^{\lambda+1}\{&(\lambda-1)\sin\big((\lambda-1)\alpha\big)\cos\big((\lambda+1)\theta\big) \\ &-(\lambda+1)\sin\big((\lambda+1)\alpha\big)\cos\big((\lambda-1)\theta\big)\} \end{aligned} \tag{12}$$

$$\begin{aligned} \phi_{S2} = Ar^{\lambda+1}\{&(\lambda+1)\cos\big((\lambda-1)\alpha\big)\cos\big((\lambda+1)\theta\big) \\ &-(\lambda+1)\cos((\lambda+1)\alpha)\cos\big((\lambda-1)\theta\big)\} \end{aligned} \tag{13}$$

$$\begin{aligned} \phi_{A1} = Ar^{\lambda+1}\{&(\lambda-1)\cos\big((\lambda-1)\alpha\big)\sin\big((\lambda+1)\theta\big) \\ &-(\lambda+1)\cos((\lambda+1)\alpha)\sin\big((\lambda-1)\theta\big)\} \end{aligned} \tag{14}$$

$$\begin{aligned} \phi_{A2} = Ar^{\lambda+1}\{&(\lambda+1)\sin((\lambda-1)\alpha)\sin\big((\lambda+1)\theta\big) \\ &-(\lambda+1)\sin((\lambda+1)\alpha)\sin\big((\lambda-1)\theta\big)\} \end{aligned} \tag{15}$$

For a given geometry we can substitute in the relevant eigenvalues to obtain the eigenvectors and therefore stress functions for each mode, as was done in Equations ((**12**-(**15)**). In this project both the crack and contact edge are being analysed, in both of these geometries $\alpha = \pi$, so we get the eigenvalues λ = 0.5,1, 1.5...etc. It can be seen that substituting into the above equations some lambda values will cause individual stress functions to become zero. If we have a value of lambda which is not a whole number i.e. 0.5, 1.5, 2.5 etcetera then cosine of alpha terms will be zero; $\phi_{S2} = \phi_{A1} = 0$. If we have the other values of 1, 2, 3 etcetera the converse is true and the sine of alpha terms become zero so

$\phi_{S1} = \phi_{A2} = 0$. So in each case there is one non-trivial solution which can be used to calculate stresses and displacements.

It should also be noted that due to the eigenvalues in the $\alpha = \pi$ case the singular terms will vary with $r^{-\frac{1}{2}}$ and so are square root singular, and the first bounded terms vary as $r^{\frac{1}{2}}$ so therefore are square root bounded. These terms will be used frequently throughout this report.

2.2 Calculating the Stresses

It is well known that we can relate stress functions to stresses in polar co-ordinates using the following equations. These may be found in lots of literature including Engineering Tables and Data[3].

$$\sigma_{rr} = \frac{1}{r}\frac{\partial \phi}{\partial r} + \frac{1}{r^2}\frac{\partial^2 \phi}{\partial \theta^2} \tag{16}$$

$$\sigma_{\theta\theta} = \frac{\partial^2 \phi}{\partial r^2} \tag{17}$$

$$\sigma_{r\theta} = -\frac{\partial}{\partial r}\left(\frac{1}{r}\frac{\partial \phi}{\partial \theta}\right) \tag{18}$$

2.2.1 Symmetric Terms

For the symmetric problem for $\alpha = \pi;\ \lambda = 0.5,1.5,2.5$ etcetera;

$$\phi_{S1} = Ar^{\lambda+1}\{(\lambda-1)\cos((\lambda+1)\theta) + (\lambda+1)\cos((\lambda-1)\theta)\} \tag{19}$$

$$\frac{\sigma_{rr}}{Ar^{\lambda-1}\sin\lambda\pi} = (\lambda^2-1)\{\cos((\lambda+1)\theta) + \cos((\lambda-1)\theta) - \lambda\cos((\lambda-1)\theta) + \lambda\cos((\lambda+1)\theta)\} + (\lambda+1)\{\cos((\lambda+1)\theta) + \cos((\lambda-1)\theta) + \lambda\cos((\lambda-1)\theta) - \lambda\cos((\lambda+1)\theta)\} \tag{20}$$

$$\frac{\sigma_{\theta\theta}}{Ar^{\lambda-1}\sin\lambda\pi} = (\lambda+1)\{\cos\big((\lambda+1)\theta\big) + \cos\big((\lambda-1)\theta\big) + \lambda\cos\big((\lambda-1)\theta\big) - \lambda\cos\big((\lambda+1)\theta\big)\} \tag{21}$$

$$\frac{2\sigma_{r\theta}}{Ar^{\lambda-1}} = \lambda(\lambda^2-1)\{\cos(\theta+\pi\lambda+\lambda\theta) + \cos(\theta+\pi\lambda-\lambda\theta) - \cos(\theta-\pi\lambda+\lambda\theta) - \cos(\theta-\pi\lambda-\lambda\theta)\} \tag{22}$$

For $\lambda = 0.5$;

$$\begin{pmatrix}\sigma_{rr}\\ \sigma_{\theta\theta}\\ \sigma_{r\theta}\end{pmatrix}^{S}_{\lambda=0.5} = \frac{A}{\sqrt{r}}\begin{pmatrix}\frac{15}{8}\cos\frac{\theta}{2} - \frac{3}{8}\cos\frac{3\theta}{2}\\ \frac{9}{8}\cos\frac{\theta}{2} + \frac{3}{8}\cos\frac{3\theta}{2}\\ \frac{3}{8}\sin\frac{\theta}{2} + \frac{3}{8}\sin\frac{3\theta}{2}\end{pmatrix} \tag{23}$$

For $\lambda = 1.5$;

$$\begin{pmatrix}\sigma_{rr}\\ \sigma_{\theta\theta}\\ \sigma_{r\theta}\end{pmatrix}^{S}_{\lambda=1.5} = A\sqrt{r}\begin{pmatrix}\frac{-45}{8}\cos\frac{\theta}{2} - \frac{15}{8}\cos\frac{5\theta}{2}\\ -\frac{75}{8}\cos\frac{\theta}{2} + \frac{15}{8}\cos\frac{5\theta}{2}\\ -\frac{15}{8}\sin\frac{\theta}{2} + \frac{15}{8}\sin\frac{5\theta}{2}\end{pmatrix} \tag{24}$$

For when $\lambda = 1$;

$$\phi_{S2} = Ar^2(2\cos(2\theta) - 2) \tag{25}$$

$$\sigma_{rr} = 4A\cos(2\theta) - 4 - 8A\cos(2\theta) = -4A(\cos(2\theta)+1) \tag{26}$$

$$\sigma_{\theta\theta} = 4A(\cos(2\theta) - 1) \tag{27}$$

$$\sigma_{r\theta} = -\frac{\partial}{\partial r}\big(-4Ar\sin(2\theta)\big) = 4A\sin(2\theta) \tag{28}$$

$$\begin{pmatrix}\sigma_{rr}\\ \sigma_{\theta\theta}\\ \sigma_{r\theta}\end{pmatrix}^{S}_{\lambda=1} = 4A\begin{pmatrix}-\cos2\theta - 1\\ \cos2\theta - 1\\ \sin2\theta\end{pmatrix} \tag{29}$$

2.2.2 *Antisymmetric Terms*

For the antisymmetric problem for $\alpha = \pi;\ \lambda = 0.5,1.5,2.5$ etcetera;

$$\phi_{A2} = r^{\lambda+1}\{(\lambda+1)\sin((\lambda-1)\alpha)\sin((\lambda+1)\theta) - (\lambda+1)\sin((\lambda+1)\alpha)\sin((\lambda-1)\theta)\} \tag{30}$$

$$\frac{-2\sigma_{rr}}{Ar^{\lambda-1}\lambda(\lambda+1)} = \cos(\theta+\pi\lambda+\lambda\theta) - 3\cos(\theta+\pi\lambda-\lambda\theta) - \cos(\theta-\pi\lambda+\lambda\theta) + 3\cos(\theta-\pi\lambda-\lambda\theta) + \lambda[\cos(\theta+\pi\lambda+\lambda\theta) + \cos(\theta+\pi\lambda-\lambda\theta) - \cos(\theta-\pi\lambda+\lambda\theta) - \cos(\theta-\pi\lambda-\lambda\theta)] \tag{31}$$

$$\frac{2\sigma_{\theta\theta}}{Ar^{\lambda-1}\lambda(\lambda+1)^2} = \cos(\theta+\pi\lambda+\lambda\theta) + \cos(\theta+\pi\lambda-\lambda\theta) - \cos(\theta-\pi\lambda+\lambda\theta) - \cos(\theta-\pi\lambda-\lambda\theta) \tag{32}$$

$$\frac{\sigma_{r\theta}}{Ar^{\lambda-1}\lambda(\lambda+1)\sin\lambda\pi} = \cos((\lambda+1)\theta) + \cos((\lambda-1)\theta) - \lambda[\cos((\lambda+1)\theta) - \cos((\lambda-1)\theta)] \tag{33}$$

For $\lambda = 0.5$;

$$\begin{pmatrix}\sigma_{rr}\\ \sigma_{\theta\theta}\\ \sigma_{r\theta}\end{pmatrix}^{A}_{\lambda=0.5} = \frac{A}{\sqrt{r}}\begin{pmatrix}\frac{-15}{8}\sin\frac{\theta}{2} + \frac{9}{8}\sin\frac{3\theta}{2}\\ -\frac{9}{8}\sin\frac{\theta}{2} - \frac{9}{8}\sin\frac{3\theta}{2}\\ \frac{3}{8}\cos\frac{\theta}{2} + \frac{9}{8}\cos\frac{3\theta}{2}\end{pmatrix} \tag{34}$$

For $\lambda = 1.5$;

$$\begin{pmatrix}\sigma_{rr}\\ \sigma_{\theta\theta}\\ \sigma_{r\theta}\end{pmatrix}^{A}_{\lambda=1.5} = A\sqrt{r}\begin{pmatrix}-\frac{45}{8}\sin\frac{\theta}{2} - \frac{75}{8}\sin\frac{5\theta}{2}\\ -\frac{75}{8}\sin\frac{\theta}{2} + \frac{75}{8}\sin\frac{5\theta}{2}\\ \frac{15}{8}\cos\frac{\theta}{2} - \frac{75}{8}\cos\frac{5\theta}{2}\end{pmatrix} \tag{35}$$

For when $\lambda = 1$;

$$\Phi_{A1} = 0 \tag{36}$$

$$\sigma_{rr} = 0\text{MPa} \tag{37}$$

$$\sigma_{\theta\theta} = 0\text{MPa} \tag{38}$$

$$\sigma_{r\theta} = 0\text{MPa} \tag{39}$$

$$\begin{pmatrix}\sigma_{rr}\\ \sigma_{\theta\theta}\\ \sigma_{r\theta}\end{pmatrix}^{A}_{\lambda=1} = A\begin{pmatrix}0\\ 0\\ 0\end{pmatrix} \tag{40}$$

2.2.3 Revised William's Solution

These terms can all be substituted into the Williams' equation. There are also scaling factors for each of the different terms (K_I, K_{II}, T, L_I, L_{II}) and so the scaling factor of A can be absorbed into these factors and therefore ignored. These scaling factors will determine the range over which each term in the series will dominate. In this project we only look at the first six terms with the intention of examining the stresses local to the crack tip or contact interface. It should be noted that if we were interested in the far field stress zone then further terms would need to be examined as higher lambda values will give larger bounded terms which may not be able to be ignored; this will of course depend on their scaling factors.

These coefficients will absorb the factor of A within them and by definition along the line $\theta = 0$ are:

$$K_I = \sigma_{\theta\theta}\sqrt{r} \to 1 \quad \boldsymbol{in\ the\ limit\ as\ r \to 0} \tag{41}$$

$$K_{II} = \sigma_{r\theta}\sqrt{r} \to 1 \quad \boldsymbol{in\ the\ limit\ as\ r \to 0} \tag{42}$$

$$T_I = \sigma_{rr} \to 1 \quad \boldsymbol{in\ the\ limit\ as\ r \to 0} \tag{43}$$

$$L_I = \frac{\sigma_{\theta\theta}}{\sqrt{r}} \to 1 \quad \boldsymbol{in\ the\ limit\ as\ r \to 0} \tag{44}$$

$$L_{II} = \frac{\sigma_{r\theta}}{\sqrt{r}} \to 1 \quad \boldsymbol{in\ the\ limit\ as\ r \to 0} \tag{45}$$

This means that the K_I, K_{II}, T, L_I, L_{II} multiplicative factors will absorb the A variable times some multiplier to allow for the above conditions to be met. In the case of the square root singular solutions this factor is $\frac{3}{2}$ for the T-Stress it is $-\frac{1}{8}$ and for the L stresses it is $\frac{15}{2}$. The first six normalised terms of the Williams solution, therefore, are as follows.

$$\begin{bmatrix}\sigma_{rr}\\ \sigma_{\theta\theta}\\ \sigma_{r\theta}\end{bmatrix} = \frac{K_I}{\sqrt{r}}\begin{pmatrix}\frac{5}{4}\cos\frac{\theta}{2} - \frac{1}{4}\cos\frac{3\theta}{2}\\ \frac{3}{4}\cos\frac{\theta}{2} + \frac{1}{4}\cos\frac{3\theta}{2}\\ \frac{1}{4}\sin\frac{\theta}{2} + \frac{1}{4}\sin\frac{3\theta}{2}\end{pmatrix} + \frac{K_{II}}{\sqrt{r}}\begin{pmatrix}\frac{-5}{4}\sin\frac{\theta}{2} + \frac{3}{4}\sin\frac{3\theta}{2}\\ -\frac{3}{4}\sin\frac{\theta}{2} - \frac{3}{4}\sin\frac{3\theta}{2}\\ \frac{1}{4}\cos\frac{\theta}{2} + \frac{3}{4}\cos\frac{3\theta}{2}\end{pmatrix} + \frac{T}{2}\begin{pmatrix}\cos2\theta + 1\\ -\cos2\theta + 1\\ -\sin2\theta\end{pmatrix}$$
$$+ L_I\sqrt{r}\begin{pmatrix}\frac{-3}{4}\cos\frac{\theta}{2} - \frac{1}{4}\cos\frac{5\theta}{2}\\ -\frac{5}{4}\cos\frac{\theta}{2} + \frac{1}{4}\cos\frac{5\theta}{2}\\ -\frac{1}{4}\sin\frac{\theta}{2} + \frac{1}{4}\sin\frac{5\theta}{2}\end{pmatrix} + L_{II}\sqrt{r}\begin{pmatrix}-\frac{3}{4}\sin\frac{\theta}{2} - \frac{5}{4}\sin\frac{5\theta}{2}\\ -\frac{5}{4}\sin\frac{\theta}{2} + \frac{5}{4}\sin\frac{5\theta}{2}\\ \frac{5}{4}\cos\frac{\theta}{2} - \frac{5}{4}\cos\frac{5\theta}{2}\end{pmatrix} \tag{46}$$

This is an important result in this thesis. These stresses are the basis for comparison between a crack tip and incomplete contact edge. The square root singular terms can be compared to the literature and found to be the same (4). The T-stress term will henceforth be ignored as it is a constant and thus the same for both situations and has no variation with r; is constant over the entire stress field. The L_{II} term we will also find is not relevant as the K_{II} term will always dominate. These stresses will be revisited and it will be further explained what terms are relevant in each scenario.

2.3 *Calculating the Displacements*

We can calculate the displacements for any given geometry and loading situation in various ways. First, we could use the stresses and through the use of Hooke's law to get plane strain equations and the relationship between strains and small displacements (3).

Plane strain equations:

$$\varepsilon_{rr} = \frac{1-\nu^2}{E}(\sigma_{rr} - \frac{\nu}{1-\nu}\sigma_{\theta\theta}) \tag{47}$$

$$\varepsilon_{\theta\theta} = \frac{1-\nu^2}{E}(\sigma_{\theta\theta} - \frac{\nu}{1-\nu}\sigma_{rr}) \tag{48}$$

Relationships between small strains and small displacements

$$\varepsilon_{rr} = \frac{\partial u}{\partial r} \tag{49}$$

$$\varepsilon_{\theta\theta} = \frac{u}{r} + \frac{\partial v}{\partial \theta} \tag{50}$$

Another way to calculate the displacements is directly from the Airy's stress function. Given that, in this case, we have already calculated the Airy's stress function the easiest way to calculate the displacements will be directly from this. Standard solutions are given in Barber's (2) book in Chapter 9.

$\boldsymbol{\phi}$	$\boldsymbol{2\mu u_r}$	$\boldsymbol{2\mu u_\theta}$	
$\boldsymbol{r^{-n+2}\cos n\theta}$	$(\kappa + n - 1)r^{-n+1}\cos n\theta$	$-(\kappa - n + 1)r^{-n+1}\sin n\theta$	(a)
$\boldsymbol{r^{n+2}\cos n\theta}$	$(\kappa - n - 1)r^{n+1}\cos n\theta$	$(\kappa + n + 1)r^{n+1}\sin n\theta$	(b)
$\boldsymbol{r^{n}\cos n\theta}$	$-nr^{n-1}\cos n\theta$	$nr^{n-1}\sin n\theta$	(c)
$\boldsymbol{r^{-n+2}\sin n\theta}$	$(\kappa + n - 1)r^{-n+1}\sin n\theta$	$(\kappa + n + 1)r^{-n+1}\cos n\theta$	(d)
$\boldsymbol{r^{n+2}\sin n\theta}$	$(\kappa - n - 1)r^{n+1}\sin n\theta$	$-(\kappa + n + 1)r^{n+1}\cos n\theta$	(e)
$\boldsymbol{r^{n}\sin n\theta}$	$-nr^{n-1}\sin n\theta$	$-nr^{n-1}\cos n\theta$	(f)

2.3.1 Symmetric Terms

For the symmetric problem for $\alpha = \pi;\ \lambda = 0.5,1.5,2.5$ etcetera;

$$\phi_{S1} = Ar^{\lambda+1}\{(\lambda-1)\sin((\lambda-1)\pi)\cos((\lambda+1)\theta) - (\lambda+1)\sin((\lambda+1)\pi)\cos((\lambda-1)\theta)\} \quad (51)$$

If $\lambda = 0.5$, we separate into two parts and use (b) with $n = -\frac{1}{2}$ and (c) with $n = \frac{3}{2}$

$$\phi_{S1} = \frac{1}{2}r^{\frac{3}{2}}\cos\left(\frac{3\theta}{2}\right) + \frac{3}{2}r^{\frac{3}{2}}\cos\left(-\frac{\theta}{2}\right) = \frac{1}{2}r^{\frac{3}{2}}\cos\left(\frac{3\theta}{2}\right) + \frac{3}{2}r^{-\frac{1}{2}+2}\cos\left(-\frac{\theta}{2}\right) \quad (52)$$

$$\begin{bmatrix}u_r\\u_\theta\end{bmatrix}^S_{K_I} = \frac{K_I}{2\mu}\begin{bmatrix}-\frac{3}{4}r^{\frac{1}{2}}\cos\frac{3\theta}{2} + \frac{3}{2}(\kappa-\frac{1}{2})r^{\frac{1}{2}}\cos\left(-\frac{\theta}{2}\right)\\ \frac{3}{4}r^{\frac{1}{2}}\sin\frac{3\theta}{2} + \frac{3}{2}(\kappa+\frac{1}{2})r^{\frac{1}{2}}\sin\left(-\frac{\theta}{2}\right)\end{bmatrix} = \frac{3r^{\frac{1}{2}}}{4}\frac{K_I}{2\mu}\begin{bmatrix}-\cos\frac{3\theta}{2} + (2\kappa-1)\cos\left(\frac{\theta}{2}\right)\\ \sin\frac{3\theta}{2} + (2\kappa+1)\sin\left(-\frac{\theta}{2}\right)\end{bmatrix} \quad (53)$$

If $\lambda = 1.5$, we separate into three parts use (b) with $n = \frac{1}{2}$ and (c) with $n = \frac{5}{2}$

$$\phi_{S1} = \frac{1}{2}r^{\frac{5}{2}}\cos\left(\frac{5\theta}{2}\right) + \frac{5}{2}r^{\frac{5}{2}}\cos\left(\frac{\theta}{2}\right) = \frac{1}{2}r^{\frac{5}{2}}\cos\left(\frac{5\theta}{2}\right) + \frac{5}{2}r^{\frac{1}{2}+2}\cos\left(\frac{\theta}{2}\right) \quad (54)$$

$$\begin{bmatrix}u_r\\u_\theta\end{bmatrix}^S_{L_I} = \begin{bmatrix}-\frac{5}{4}r^{\frac{3}{2}}\cos\frac{3\theta}{2} + (\kappa-\frac{3}{2})r^{\frac{3}{2}}\cos\frac{\theta}{2}\\ \frac{5}{2}r^{\frac{3}{2}}\sin\frac{5\theta}{2} + (\kappa+\frac{3}{2})r^{\frac{3}{2}}\sin\frac{\theta}{2}\end{bmatrix} = \frac{5r^{\frac{3}{2}}L_I}{8\mu}\begin{bmatrix}-\cos\frac{5\theta}{2} + (2\kappa-3)\cos\frac{\theta}{2}\\ 5\sin\frac{5\theta}{2} + (2\kappa+3)\sin\frac{\theta}{2}\end{bmatrix} \quad (55)$$

To verify this method of calculating the displacements we can compare the square root singular solutions to those found in literature. The solution given in the book 'Fracture of Brittle Solids'[4] is as follows:

$$\begin{bmatrix} u_r \\ u_\theta \end{bmatrix}_{K_I}^{S} = \frac{K_I}{2E}\left(\frac{r}{2\pi}\right)^{\frac{1}{2}} \begin{bmatrix} (1+\nu)\left((2\kappa-1)\cos\frac{\theta}{2} - \cos\frac{3\theta}{2}\right) \\ (1+\nu)\left(-(2\kappa+1)\sin\frac{\theta}{2} + \sin\frac{3\theta}{2}\right) \end{bmatrix} \tag{56}$$

By substituting in $\mu = \frac{E}{2(1+\nu)}$ into Equation (**53** and simplifying:

$$\begin{bmatrix} u_r \\ u_\theta \end{bmatrix}_{K_I}^{S} = \frac{(1+\nu)}{2E}\frac{3r^{\frac{1}{2}}}{2} \begin{bmatrix} -\cos\frac{3\theta}{2} + (2\kappa-1)\cos\frac{\theta}{2} \\ \sin\frac{3\theta}{2} - (2\kappa+1)\sin\frac{\theta}{2} \end{bmatrix} \tag{57}$$

This shows that the method is correct, there is a factor of difference. Sometimes the $\left(\frac{1}{2\pi}\right)^{\frac{1}{2}}$ multiplier is included and sometimes it isn't, it depends on which text book/paper you read.

The factor of $\frac{3}{2}$ is due to the normalisation of the stresses to fit the standard model, this can be seen from the fact that the stresses in Equation (23) have the same factor of difference. Therefore we will also normalise the displacements with the factors calculated in Section 2.2.3.

$$\begin{bmatrix} u_r \\ u_\theta \end{bmatrix}_{K_I}^{S} = \frac{r^{\frac{1}{2}}}{2}\frac{K_I}{2\mu} \begin{bmatrix} -\cos\frac{3\theta}{2} + (2\kappa-1)\cos\left(\frac{\theta}{2}\right) \\ \sin\frac{3\theta}{2} + (2\kappa+1)\sin\left(-\frac{\theta}{2}\right) \end{bmatrix} \tag{58}$$

$$\begin{bmatrix} u_r \\ u_\theta \end{bmatrix}_{L_I}^{S} = \frac{r^{\frac{3}{2}}L_I}{12\mu} \begin{bmatrix} -\cos\frac{5\theta}{2} + (2\kappa-3)\cos\frac{\theta}{2} \\ 5\sin\frac{5\theta}{2} + (2\kappa+3)\sin\frac{\theta}{2} \end{bmatrix} \tag{59}$$

2.3.2 Antisymmetric Terms

For the antisymmetric problem for $\alpha = \pi$; $\lambda = 0.5, 1.5, 2.5$ etcetera. However the only term we will be interested in is the square root singular one. This can be obtained in a normalised form from literature but will be calculated here to ensure consistency and that the correct multiplier is used.

$$\Phi_{A2} = r^{\lambda+1}\{(\lambda+1)\sin((\lambda-1)\alpha)\sin((\lambda+1)\theta) - (\lambda+1)\sin((\lambda+1)\alpha)\sin((\lambda-1)\theta)\} \quad (60)$$

If $\lambda = 0.5$, we separate into two parts and use (e) with $n = -\frac{1}{2}$ and (f) with $n = \frac{3}{2}$

$$\Phi_{A2} = -\frac{3}{2}r^{\frac{3}{2}}\sin\frac{3\theta}{2} + \frac{3}{2}r^{\frac{3}{2}}\sin\left(-\frac{\theta}{2}\right) = -\frac{3}{2}r^{\frac{3}{2}}\sin\frac{3\theta}{2} + \frac{3}{2}r^{-\frac{1}{2}+2}\sin\left(-\frac{\theta}{2}\right) \quad (61)$$

$$\begin{bmatrix}u_{rr}\\u_{\theta\theta}\end{bmatrix}^{A}_{K_{II}} = \frac{K_{II}}{2\mu}\begin{bmatrix}\frac{9}{4}r^{\frac{1}{2}}\sin\frac{3\theta}{2} + \frac{3}{2}(\kappa-\frac{1}{2})r^{\frac{1}{2}}\sin\left(-\frac{\theta}{2}\right)\\ \frac{9}{4}r^{\frac{1}{2}}\cos\frac{3\theta}{2} - \frac{3}{2}(\kappa+\frac{1}{2})r^{\frac{1}{2}}\cos\left(-\frac{\theta}{2}\right)\end{bmatrix} = \frac{3r^{\frac{1}{2}}}{4}\frac{K_{II}}{2\mu}\begin{bmatrix}3\sin\frac{3\theta}{2} - (2\kappa-1)\sin\frac{\theta}{2}\\ 3\cos\frac{3\theta}{2} - (2\kappa+1)\cos\frac{\theta}{2}\end{bmatrix} \quad (62)$$

This displacement equation can also be shown to be identical besides a multiplicative factor to that in 'Fracture of Brittle Solids' [4]. The stresses and displacements calculated in this section may be applied to a model to give the desired stress field. This can be done either purely analytically using elasticity and violations, through finite element analysis using elasticity and violations or through finite element analysis including plasticity and allowing for the redistribution of stresses due to the yielded region.

$$\begin{bmatrix}u_r\\u_\theta\end{bmatrix}^{A}_{K_{II}} = \frac{r^{\frac{1}{2}}}{2}\frac{K_{II}}{2\mu}\begin{bmatrix}3\sin\frac{3\theta}{2} - (2\kappa-1)\sin\frac{\theta}{2}\\ 3\cos\frac{3\theta}{2} - (2\kappa+1)\cos\frac{\theta}{2}\end{bmatrix} \quad (63)$$

2.4 *Size of the Yielded Region*

In this section the expected size of the plasticity zone will be calculated for set angles. The reason for this is so to ensure when models are made they can be checked against the known solution in the

first instance. The results in this section will later be used in the Abaqus (the finite element package used) analysis.

An estimate for the size of the yielded region can be formed based on violations of Von Mises' yield condition. The larger the plastic zone the more inaccurate this estimation will be. We already have equations for the stresses in plane polar co-ordinates. If the material is in plane strain with Poisson's ratio *v*, the through thickness stress is

$$\sigma_{zz} = \nu(\sigma_{rr} + \sigma_{\theta\theta}) \tag{64}$$

Given the material has yield strength in pure shear *k* then the yield condition is given by:

$$(\sigma_{rr} - \sigma_{\theta\theta})^2 + (\sigma_{\theta\theta} - \sigma_{zz})^2 + (\sigma_{zz} - \sigma_{rr})^2 + 6{\sigma_{r\theta}}^2 = 6k^2 \tag{65}$$

If we look, first, at the crack-tip problem we can write down the state of stress in contracted form as

$$\sigma_{ij}(r,\theta) = \frac{K_I}{\sqrt{r}} f_{ij}^{I}(\theta) + \frac{K_{II}}{\sqrt{r}} f_{ij}^{II}(\theta) \tag{66}$$

Therefore substituting this into the equation for Von Mises yield criterion. We can find the plastic radius, $r_p(\theta)$, for any given combination of stress intensity factors (K_I and K_{II}) by finding the radius at yield.

$$\begin{aligned} 6r_p k^2 = {} & (K_I f_{rr}^{I} + K_{II} f_{rr}^{II} - K_I f_{\theta\theta}^{I} - K_{II} f_{\theta\theta}^{II})^2 + (K_I f_{\theta\theta}^{I} + K_{II} f_{\theta\theta}^{II} - K_I f_{zz}^{I} - K_{II} f_{zz}^{II})^2 \\ & + (K_I f_{zz}^{I} + K_{II} f_{zz}^{II} - K_I f_{rr}^{I} - K_{II} f_{rr}^{II})^2 + 6(K_I f_{r\theta}^{I} + K_{II} f_{r\theta}^{II})^2 \end{aligned} \tag{67}$$

Which can be simplified to

$$\frac{r_p k^2}{{K_I}^2} = \frac{1}{6}\Big[(f_{rr}^I + \frac{K_{II}}{K_I} f_{rr}^{II} - f_{\theta\theta}^I - \frac{K_{II}}{K_I} f_{\theta\theta}^{II})^2 + (f_{\theta\theta}^I + \frac{K_{II}}{K_I} f_{\theta\theta}^{II} - f_{zz}^I - \frac{K_{II}}{K_I} f_{zz}^{II})^2 + (f_{zz}^I + \frac{K_{II}}{K_I} f_{zz}^{II} - f_{rr}^I - \frac{K_{II}}{K_I} f_{rr}^{II})^2\Big] + (f_{r\theta}^I + \frac{K_{II}}{K_I} f_{r\theta}^{II})^2 \quad (68)$$

So, a plot of the right hand side of this equation, taking $\frac{K_{II}}{K_I}$as a parameter, will display the normalised shape of the crack tip plasticity zones. Note that we are defining the stress intensity factors, here, without the customary $\sqrt{2\pi}$ factor.

The expected size of the plastic radius for any given yield stress may be calculated. To check the accurateness of the finite element model we will calculate the size of the yield zone for the individual modes. We know that the expected shape of single mode I and mode II stress fields are as shown in the Figure 2 below.

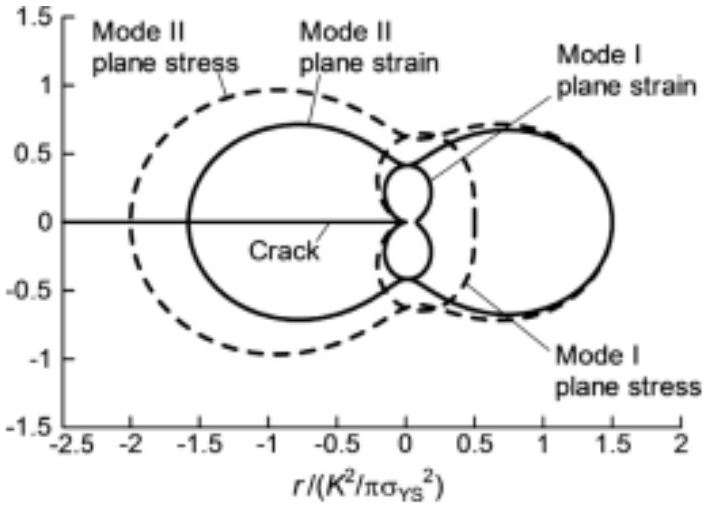


Figure 2 - A plot showing the difference between the symmetric and antisymmetric stress fields for the square root singular terms in both plane stress and plane strain[5]

2.4.1 Mode I

We know mode I is expected to be a figure eight shape in plane strain.

We are using a Von Mises stress criterion (note here we are not using the pure shear yield condition as before) to plot the stress field and hence find the plastic radius for a given yield stress.

$$2\sigma_y^2 = (\sigma_{xx} - \sigma_{yy})^2 + (\sigma_{yy} - \sigma_{zz})^2 + (\sigma_{zz} - \sigma_{xx})^2 + 6({\sigma_{xy}}^2 + {\sigma_{yz}}^2 + {\sigma_{xz}}^2) \quad (69)$$

In polar co-ordinates with the only shear force being in the $r\theta$ direction this simplifies to.

$$2\sigma_y^2 = (\sigma_{rr} - \sigma_{\theta\theta})^2 + (\sigma_{\theta\theta} - \sigma_{zz})^2 + (\sigma_{zz} - \sigma_{rr})^2 + 6{\sigma_{r\theta}}^2 \quad (70)$$

Where (if $\nu = 0.3$) and the material is behaving purely elastically

$$\sigma_{zz} = 0.3(\sigma_{rr} + \sigma_{\theta\theta}) \quad (71)$$

Therefore the mode I stresses are (4):

$$\begin{Bmatrix} \sigma_{rr} \\ \sigma_{\theta\theta} \\ \sigma_{r\theta} \end{Bmatrix} = \frac{K_I}{(2\pi r)^{\frac{1}{2}}} \begin{Bmatrix} \cos\frac{\theta}{2}\left[1 + \sin^2\frac{\theta}{2}\right] \\ \cos^3\frac{\theta}{2} \\ \sin\frac{\theta}{2}\cos^2\frac{\theta}{2} \end{Bmatrix} \quad (72)$$

On the line θ = 0 the mode I stresses are

$$\begin{Bmatrix} \sigma_{rr} \\ \sigma_{\theta\theta} \\ \sigma_{r\theta} \end{Bmatrix} = \frac{K_I}{(2\pi r)^{\frac{1}{2}}} \begin{Bmatrix} 1 \\ 1 \\ 0 \end{Bmatrix} \quad (73)$$

$$\sigma_{zz} = \frac{0.3K_I}{(2\pi r)^{\frac{1}{2}}}(1 + 1) = \frac{0.6K_I}{(2\pi r)^{\frac{1}{2}}} \quad (74)$$

Therefore through the use of the Von Mises yield parameter we can form a relation between the plastic radius, yield stress and stress intensity factor at $\theta = 0$ as follows:

$$\sigma_y \frac{(2\pi r_p)^{\frac{1}{2}}}{K_I} = \frac{1}{\sqrt{2}}[(1-1)^2 + (1-0.6)^2 + (0.6-1)^2]^{\frac{1}{2}} = 0.4 \tag{75}$$

On the line $\theta = \frac{\pi}{2}$ mode I stresses give

$$\begin{Bmatrix} \sigma_{rr} \\ \sigma_{\theta\theta} \\ \sigma_{r\theta} \end{Bmatrix} = \frac{K_I}{(2\pi r)^{\frac{1}{2}}} \begin{Bmatrix} \cos\frac{\theta}{2}\left[1 + \sin^2\frac{\theta}{2}\right] \\ \cos^3\frac{\theta}{2} \\ \sin\frac{\theta}{2}\cos^2\frac{\theta}{2} \end{Bmatrix} = \frac{K_I}{(2\pi r)^{\frac{1}{2}}} \begin{Bmatrix} \frac{\sqrt{2}}{2}\left[1 + \frac{\sqrt{2}}{2}\frac{\sqrt{2}}{2}\right] \\ \frac{\sqrt{2}}{2}\frac{\sqrt{2}}{2}\frac{\sqrt{2}}{2} \\ \frac{\sqrt{2}}{2}\frac{\sqrt{2}}{2}\frac{\sqrt{2}}{2} \end{Bmatrix} = \frac{K_I}{(2\pi r)^{\frac{1}{2}}} \begin{Bmatrix} \frac{3\sqrt{2}}{4} \\ \frac{\sqrt{2}}{4} \\ \frac{\sqrt{2}}{4} \end{Bmatrix} \tag{76}$$

Therefore if no plastic strains are present

$$\sigma_{zz} = \frac{K_I}{(2\pi r)^{\frac{1}{2}}} 0.3\left(\frac{3\sqrt{2}}{4} + \frac{\sqrt{2}}{4}\right) = \frac{K_I}{(2\pi r)^{\frac{1}{2}}} \frac{3\sqrt{2}}{10} \tag{77}$$

Therefore through the use of the Von Mises yield parameter we can form a relation between the plastic radius, yield stress and stress intensity factor at $\theta = \frac{\pi}{2}$ as follows:

$$\sigma_y \frac{(2\pi r_p)^{\frac{1}{2}}}{K_I} = \frac{1}{\sqrt{2}}\left[\left(\frac{3\sqrt{2}}{4} - \frac{\sqrt{2}}{4}\right)^2 + \left(\frac{\sqrt{2}}{4} - \frac{3\sqrt{2}}{10}\right)^2 + \left(\frac{3\sqrt{2}}{10} - \frac{3\sqrt{2}}{4}\right)^2 + 6\left(\frac{\sqrt{2}}{4}\right)^2\right]^{\frac{1}{2}} = 0.911 \tag{78}$$

2.4.2 Mode II

In mode II loading we know that the shape of the yield surface will be like a figure eight rotated by $\frac{\pi}{2}$.

The mode II stresses are given as (4)

$$\begin{Bmatrix}\sigma_{rr}\\ \sigma_{\theta\theta}\\ \sigma_{r\theta}\end{Bmatrix} = \frac{K_{II}}{(2\pi r)^{\frac{1}{2}}}\begin{Bmatrix}\sin\frac{\theta}{2}\left[1-3\sin^2\frac{\theta}{2}\right]\\ -3\sin\frac{\theta}{2}\cos^2\frac{\theta}{2}\\ \cos\frac{\theta}{2}\left[1-3\sin^2\frac{\theta}{2}\right]\end{Bmatrix} \tag{79}$$

Substituting in $\theta = 0$

$$\begin{Bmatrix}\sigma_{rr}\\ \sigma_{\theta\theta}\\ \sigma_{r\theta}\end{Bmatrix} = \frac{K_{II}}{(2\pi r)^{\frac{1}{2}}}\begin{Bmatrix}0\\ 0\\ 1\end{Bmatrix} \tag{80}$$

$$\sigma_{zz} = \frac{K_I}{(2\pi r)^{\frac{1}{2}}}(0) = 0 \tag{81}$$

Therefore through the use of the Von Mises yield parameter we can form a relation between the plastic radius, yield stress and stress intensity factor at $\theta = 0$ as follows:

$$\sigma_y\frac{(2\pi r_p)^{\frac{1}{2}}}{K_{II}} = \frac{1}{\sqrt{2}}[(0)^2+(0)^2+(0)^2+6(1)^2]^{\frac{1}{2}} = \sqrt{3} = 1.73 \tag{82}$$

Or on the line $\theta = \frac{\pi}{2}$ gives

$$\begin{Bmatrix}\sigma_{rr}\\ \sigma_{\theta\theta}\\ \sigma_{r\theta}\end{Bmatrix} = \frac{K_{II}}{(2\pi r)^{\frac{1}{2}}}\begin{Bmatrix}\frac{\sqrt{2}}{2}\left[1-3\frac{\sqrt{2}}{2}\frac{\sqrt{2}}{2}\right]\\ -3\frac{\sqrt{2}}{2}\frac{\sqrt{2}}{2}\frac{\sqrt{2}}{2}\\ \frac{\sqrt{2}}{2}\left[1-3\frac{\sqrt{2}}{2}\frac{\sqrt{2}}{2}\right]\end{Bmatrix} = \frac{K_{II}}{(2\pi r)^{\frac{1}{2}}}\begin{Bmatrix}-\frac{\sqrt{2}}{4}\\ -3\frac{3\sqrt{2}}{4}\\ -\frac{\sqrt{2}}{4}\end{Bmatrix} \tag{83}$$

$$\sigma_{zz} = 0.3\left(-\frac{\sqrt{2}}{4}-\frac{3\sqrt{2}}{4}\right) = -\frac{3\sqrt{2}}{10}\text{MPa} \tag{84}$$

Therefore through the use of the Von Mises yield parameter we can form a relation between the plastic radius, yield stress and stress intensity factor at $\theta = \frac{\pi}{2}$ as follows:

$$\sigma_y \frac{(2\pi r_p)^{\frac{1}{2}}}{K_I} = \frac{1}{\sqrt{2}}\left[\left(-\frac{\sqrt{2}}{4}+\frac{3\sqrt{2}}{4}\right)^2+\left(-\frac{3\sqrt{2}}{4}+\frac{3\sqrt{2}}{10}\right)^2+\left(-\frac{\sqrt{2}}{4}+\frac{3\sqrt{2}}{10}\right)^2+6\left(\frac{\sqrt{2}}{4}\right)^2\right]^{\frac{1}{2}} \quad (85)$$

$$= 0.911$$

These equations will be revisited later in this report to validate the finite element model created.

3 *Elastic Analysis: Giannakopoulos' Innovation [6]*

Giannakopoulos has previously studied the similarities between a complete contact and crack tip, his research will be discussed in this section and its relevance to the incomplete contact and crack tip comparison which will be undertaken.

An important contribution to the crack tip vs. contact edge similarities debate was made by Giannakopolous in the 1990s [6]. It drew similarities between a contact edge for the geometry of the complete contact between a punch and a half plane as shown on the left of Figure 3; and two crack tips, as shown on the right. This analysis was done in the context of assuming that the square root singular terms from the Williams' solution (which is discussed more fully in Section 2) dominate both cases in both symmetric and antisymmetric loading, and in both configurations. But, in the case of the contact problem (Figure 3(1)), this would require the 'punch' to be rigid and the corresponding half-plane to be comprised of an incompressible material (Poisson's ratio of ½). Note that the punch simply becomes a quarter plane when we zoom in to the corner, and the geometry becomes increasingly self-similar in character. These incompressibility and rigid simplifications are not actually accurate for real life engineering problems.

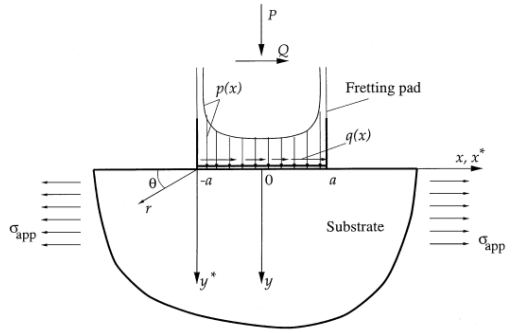


Fig. 1. A schematic representation of the contact between a two-dimensional rectangular punch and a substrate. The normal and shear loading at the contact interface and the external loading of the substrate are also indicated.

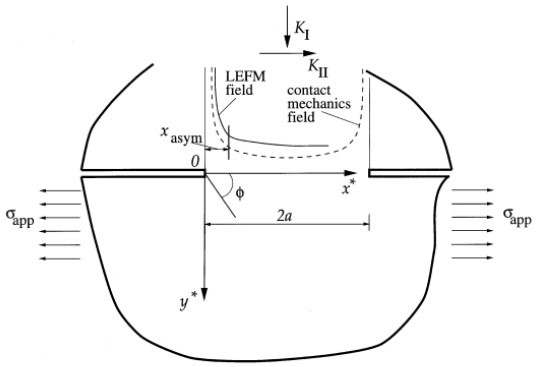


Fig. 2. Crack analogue of Fig. 1 showing the double-edge cracked plate specimen which is subjected to mode I and mode II stress intensity factors, K_I and K_{II}.

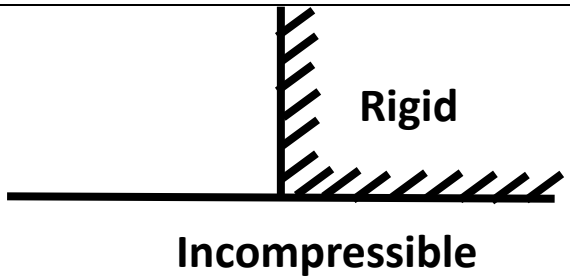
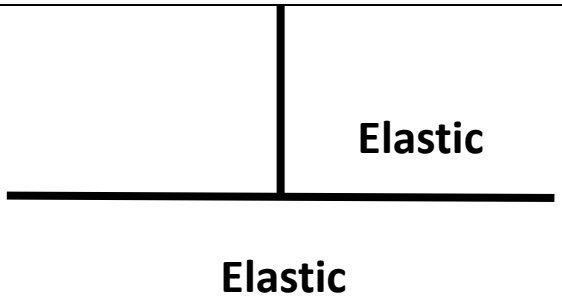
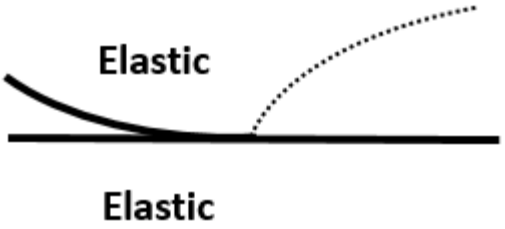
Figure 3 - Figures from Giannakopolous' Paper [6]

The work of Giannakopolous, although pioneering at the time can now be recognised to have various simplifying assumptions. The approach to comparing the contact edge and crack tip must be more rigorous than the model proposed by Giannakopolous.

It is commonly contested whether the two problems; (a) tip of a crack and (d) two contacting bodies with a high enough coefficient of friction to prevent all slip represent the same situation at the edge. In the case (a) of the crack we can have both mode one and mode two square root singular terms to represent the singularity, and note that the mode *I* loading is conventionally tensile so that the faces open up. However, for the incomplete contact problem, mode one symmetric, square root singular loading cannot be present, as the contact pressure is known to smoothly go to zero as the edge is approached; and it is compressive because the interface can support no tension. The square root singular solution would, of course give an infinitely large stress at the crack tip which is physically unrealistic. Therefore, the symmetric, square root bounded, solution will be the dominant symmetric one in the case of the contacting bodies, together with the square root singular antisymmetric term, which represents the character of the shear mode loading problem if all slip is inhibited. This will mean the K_{II} (antisymmetric, square root singular) solution will dominate and cause a plasticity zone similar to the crack tip, and then the L_I solution (symmetric, square root bounded, term from Williams' solution) will dominate as the radius tends to infinity and cause a second plasticity zone. The result will be a two plastic zones with an elastic 'band' between them; only the inner plastic region is of physical relevance.

There are four different geometries and therefore stress states to be aware of here. This thesis is based around the comparison of (a) and (d).

Table 1 – A table to show different geometries and the corresponding contributors to the size of the plastic zone

(a) Crack Tip		Square root singular – K_I and $K_{II.}$ $K_I > 0$
(b) Perfect Complete Contact as analysed by Giannakopolous		Square root singular – K_I and $K_{II.}$ $K_I < 0$
(c) Elastic Complete Contact		Singular but not necessarily as square root. Depends on geometry from Williams' solution. $\sigma_{ij} \sim r^{\lambda-1}$ Where $\lambda > {}^{1}/_{2}$
(d) Elastic Incomplete Contact		Square root bounded symmetric L_I term. Square root singular antisymmetric K_{II} term. $L_I < 0$

4 *Elastic Analysis: The No-Slip Edge Condition*

In order to use an assumption of a fully stuck contact we need to ensure that the no slip edge condition is met. This section is used to show how we may verify this for given geometry and loading conditions. It will then later be referred back to once the size of the plastic zone has been established.

There are two different plasticity zones in the incomplete contact case; one at the crack tip from the singular K_{II} and one at far field stresses due to the bounded (i.e. increases to infinite as radius does) L_I term – the latter is irrelevant and relates to a region in which the asymptotic form does not apply. For a weak (low yield strength) material, the inner plastic zone – the one of relevance in this study, might envelope the whole of the local slip region as shown in the right hand figure (Figure 4). In this case the presence of the slip region is likely to be irrelevant compared with a homogenous body, or, at any rate, to have only a trivial effect. If the material is very strong (high yield strength) the plastic zone might very well be localised at the stick-slip boundary (left hand diagram, Figure 4), in which case the presence of the slip region will make the problem rather different from that in a homogeneous body.

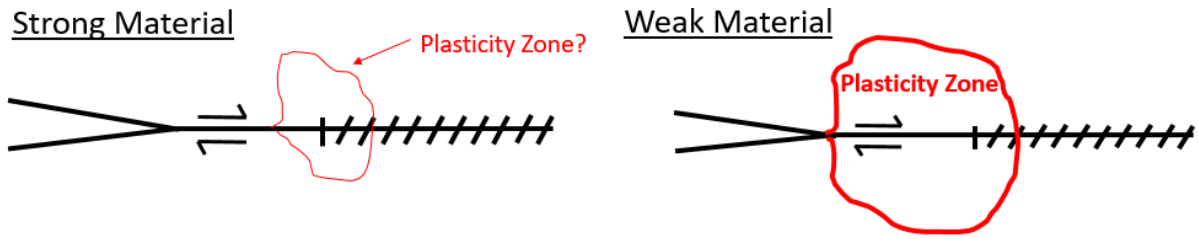


Figure 4 - Difference between stress fields in weak and strong materials

In this analysis, we assume a high enough coefficient of friction to inhibit all frictional slip. It can be seen from this Figure 5 that as we take the coefficient of friction to a high value we find the frictional slip zone is very small. In the contact problem, frictional slip will only have an effect on the stress if it is acting over a larger area than the plastic slip, as noted above. We can, once we have completed the

analysis and know the plastic zone sizes, apply realistic coefficients of friction and if the frictional slip zone remains inside the plasticity zone then the fully stuck contact can be proven to be appropriate.

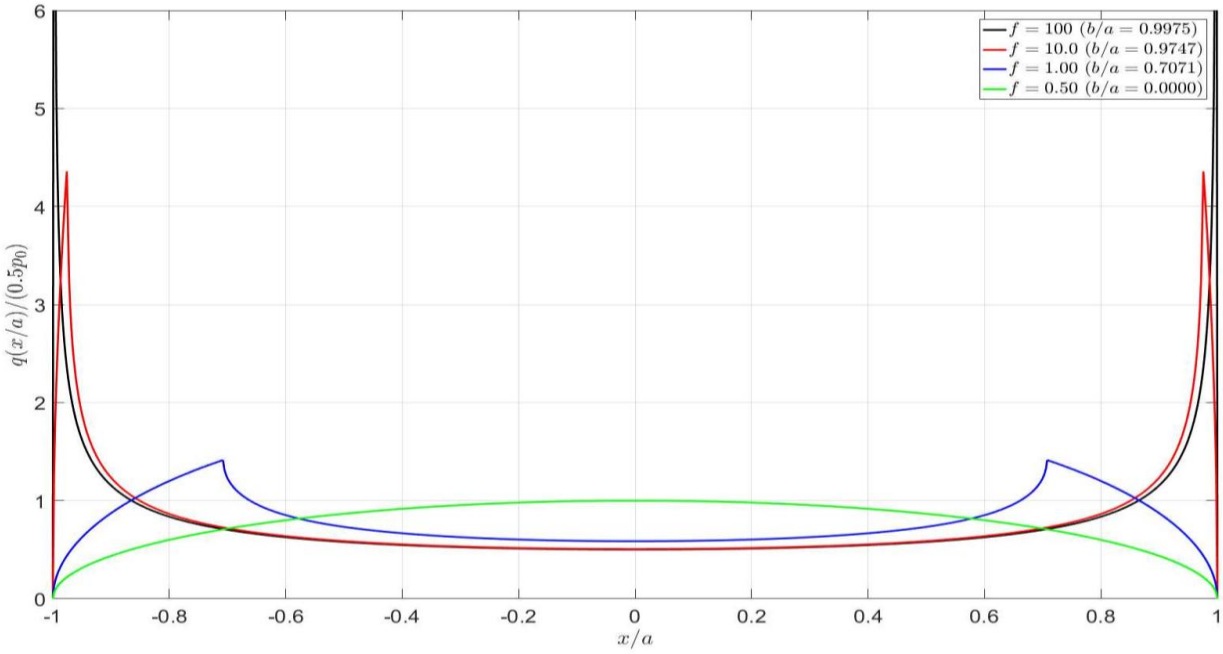


Figure 5 - The size of frictional slip zones at different coefficients of friction.

In Figure 5 the variable '*a*' is the half width of the contact and the variable '*b*' is the half width of the fully stuck portion. The variable *'q'* is the shear pressure, *'x'* is the distance from the centre of the contact and *'p_0'* is the normal pressure applied.

5 *Elastic Analysis: Mode Mixity in Contact Edge Geometry*

In the case of a mix of singular and bounded solutions we note that the solutions will not be self-similar for different values of *r* (as is true for the crack tip). This section looks at how we can sensibly scale the different solutions in a way which is physically significant.

It is assumed that the contact friction is sufficiently high to inhibit all slip at the contact edge, and that the local state of stress is captured by the square root bounded normal (symmetric) asymptote and the singular shear (antisymmetric) asymptote so that

$$\sigma_{ij}(r,\theta) = L_I\sqrt{r}h_{ij}^{I}(\theta) + \frac{K_{II}}{\sqrt{r}}f_{ij}^{II}(\theta) \tag{86}$$

Because the (generalised) stress intensity factors have dimensions of K_{II} [FL$^{-3/2}$] and L_I [FL$^{-5/2}$] careful consideration of how to combine these factors and what they physically mean is needed. It should be noted here that, on the other hand, the solution for a crack is self-similar as the K_I and K_{II} values have the same dimensions. In order to non-dimensionalise *the incomplete contact* interface case we must choose two new independent parameters to characterise the solution, say

$$d_0 = \frac{K_{II}}{L_I} \quad [L] \tag{87}$$

$$H_0 = \sqrt{L_I K_{II}} \quad [FL^{-2}] \tag{88}$$

These two new variables allow us to define a non-dimensional stress and a non-dimensional plastic radius, which permit us to collocate the solution found into many different loading cases and geometries.

$$Non-Dimensional\ Plastic\ Radius = \frac{r_p}{d_0} \tag{89}$$

$$Non - Dimensional\ Yield\ Stress = \frac{\sigma_y}{H_0} \tag{90}$$

This therefore means that we can now write the state of stress in the form

$$\frac{\sigma_{ij}(r,\theta)}{H_0} = \sqrt{\frac{r}{d_0}} h_{ij}^{I}(\theta) + \sqrt{\frac{d_0}{r}} f_{ij}^{II}(\theta) \tag{91}$$

This provides the framework for the display of plasticity zones in a novel way which will incorporate mode mixity. The dimensionless plastic radius $\frac{r_p(\theta)}{d_0}$is given by substituting into the below equation.

$$(\sigma_{rr} - \sigma_{\theta\theta})^2 + (\sigma_{\theta\theta} - \sigma_{zz})^2 + (\sigma_{zz} - \sigma_{rr})^2 + 6{\sigma_{r\theta}}^2 = 6k^2 \tag{92}$$

Which becomes

$$\begin{aligned} 6\left(\frac{k}{H_0}\right)^2 = &\left(\sqrt{\frac{r_p}{d_0}}\left(h_{rr}^{I}(\theta) - h_{\theta\theta}^{I}(\theta)\right) + \sqrt{\frac{d_0}{r_p}}\left(f_{rr}^{II}(\theta) - f_{\theta\theta}^{II}(\theta)\right)\right)^2 \\ &+ \left(\sqrt{\frac{r_p}{d_0}}\left(h_{\theta\theta}^{I}(\theta) - h_{zz}^{I}(\theta)\right) + \sqrt{\frac{d_0}{r_p}}\left(f_{\theta\theta}^{II}(\theta) - f_{zz}^{II}(\theta)\right)\right)^2 \\ &+ \left(\sqrt{\frac{r_p}{d_0}}\left(h_{zz}^{I}(\theta) - h_{rr}^{I}(\theta)\right) + \sqrt{\frac{d_0}{r_p}}\left(f_{zz}^{II}(\theta) - f_{rr}^{II}(\theta)\right)\right)^2 \\ &+ 6\left(\sqrt{\frac{r_p}{d_0}} h_{r\theta}^{I}(\theta) + \sqrt{\frac{d_0}{r_p}} f_{r\theta}^{II}(\theta)\right)^2 \end{aligned} \tag{93}$$

This is clearly a rather ‘nastier’ thing to plot because r_p/d_0 appears in both ’right way up’ and reciprocal forms. Also, it is clear that there are two plastic regions, one near the origin and one remote,

with an elastic band (as it were) between. We are interested only in the smaller (inner) region. The best way to tackle this will be to invert the dependent and independent variables, i.e. to pick, for any θ, the value of r_p/d_0 and to find the corresponding value of H_0/k. Eventually we want contours of the shape of the inner r_p/d_0 as a function of H_0/k. This is plotted out in Section 6.2.

6 *Elastic Analysis: Results*

6.1 Crack Tip

It is common knowledge and has been shown multiple times that the shape of the plastic zone in plane strain for a crack tip is as shown in Figure 6. The crack is on the right hand side and the red dotted line shows the bisector.

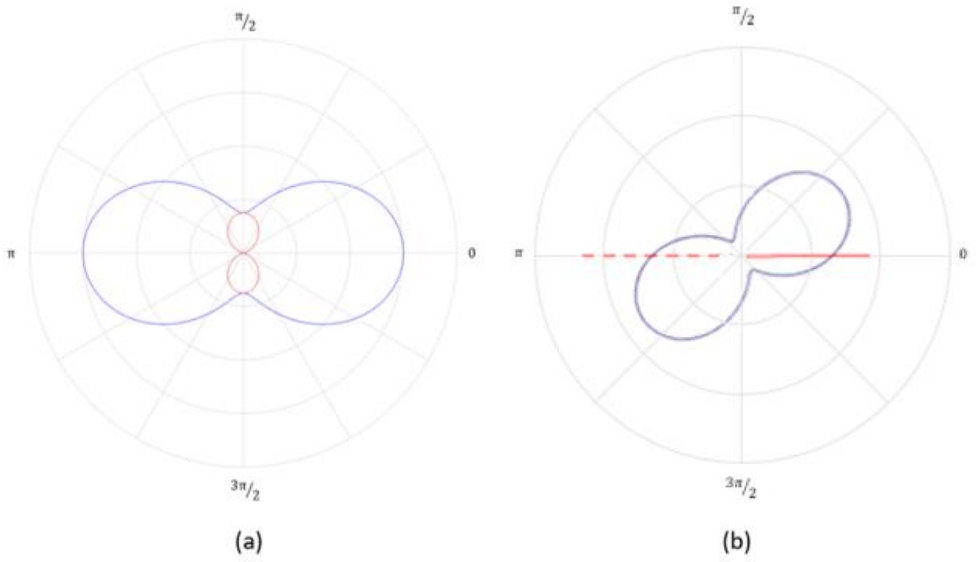


Figure 6 – Plastic radii for a crack tip in singular mode one and mode two loading

6.2 Incomplete Contact Interface

In the contact case, as previously stated, it is expected to have two plastic zones with an 'elastic band' between them. The first plastic zone is formed at the crack tip and caused by the square root singular mode II (shearing) term. The second, far field plastic zone, is caused by the square root bounded symmetric term. It should also be noted that the other bounded terms might have an effect on the far field plasticity zone it will depend on the size of the relative scaling factors applied to each term (i.e. the size of L_I etc).

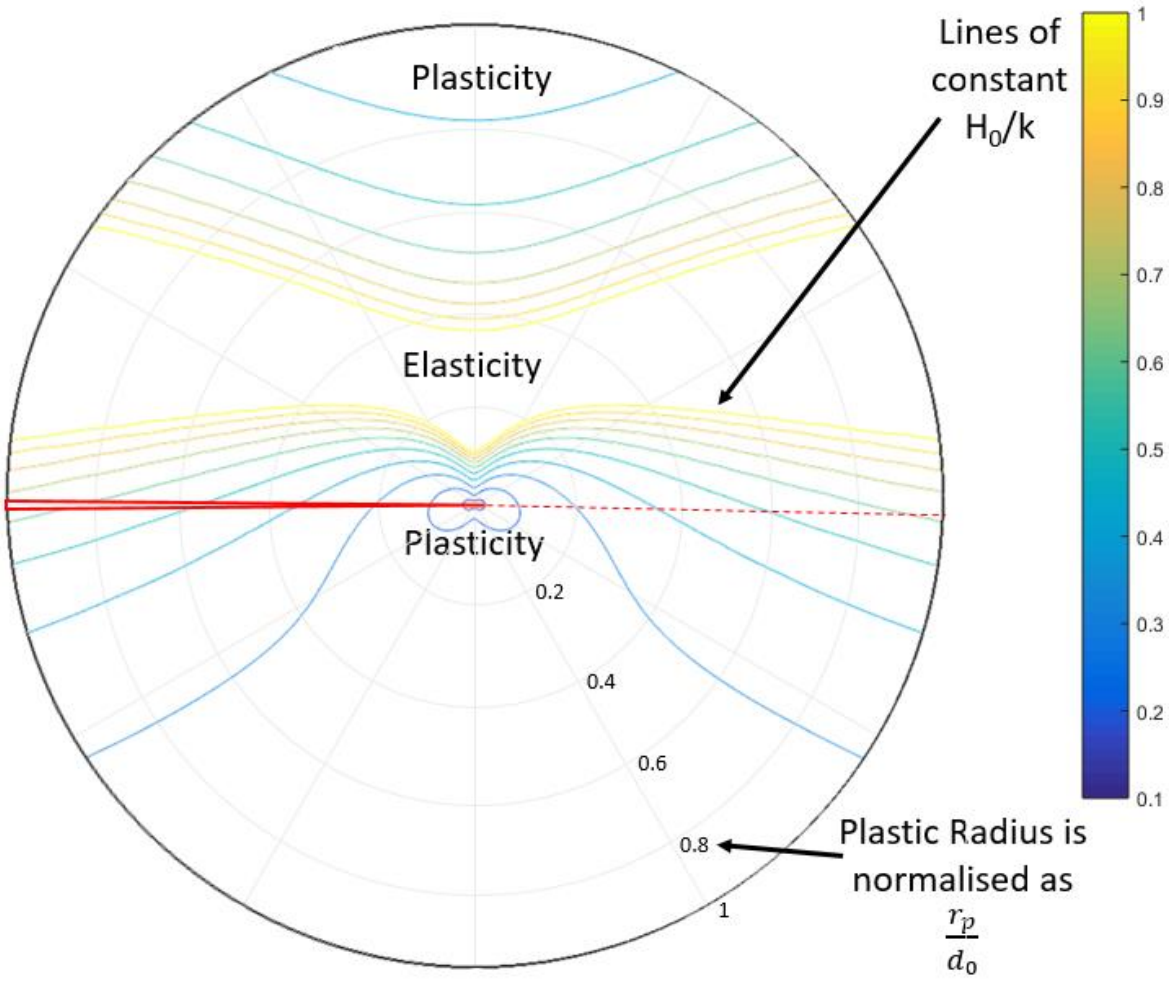


Figure 7 – Stress field for a contact interface with singular mode 2 and bounded mode 1 (K_{II} and L_I)

This plot shows the dimensionless plastic radius on the *r* axes and has contours of constant dimensionless yield stress in pure shear. The plasticity zones are obviously not similar, and more detailed plastic analysis is required to investigate the similarities between these two geometries.

7 *Plastic Analysis: Plastic Shakedown*

It has been shown that the analytical analysis using elasticity and violations of the Von Mises yield criterion do not reveal a similar plastic zone for the crack tip and contact interface. However, this doesn't mean that in real engineering applications they won't *become* similar after a number of cycles of loading. The analytical analysis is done using elasticity and violations; that is to say that the redistribution of stresses is not accounted for. This method can be relatively accurate with small plastic zones but in this case it is believed that a more thorough approach of looking at plasticity using Finite Element Analysis is needed to draw any realistic conclusions. Therefore, a model was made and this computational analysis comprises the second section of this thesis. The premise is that in both cases we have the same antisymmetric loading (the K_{II}), and therefore by applying a constant K_I or L_I load and oscillating the K_{II} it may be seen that the K_{II} loading shakes down the L_I and K_I loading, giving us the same residual plastic zone.

The behaviour of materials can vary dramatically in the plastic regime. Plastic hardening may occur, which can be either isotropic or kinematic. Isotropic hardening is when the yield surface of a material will expand and therefore there is an increase in the yield stress. Kinematic hardening is when the yield surface remains the same size and shape but moves with respect to the origin of the zero stress state. Isotropic hardening is seen in cyclic loading as the yield surface increases in size in all directions, however kinematic hardening is only seen in loading in a single direction as kinematic hardening in a positive loading cycle will mean that the material goes plastic more quickly in a negative loading cycle.

Hardening is a change in the yield surface due to an increased hindrance to dislocation glide, shakedown is different in that it is due to residual stresses and is caused by the origin of the yield surface moving; rather than the yield surface itself. Melan's Theorem [7] states that a structure shakes down if a stress field exists which can exist entirely in the elastic envelope. It is seen that if there exists a movement of the yield surface which a given loading cycle can fit within the yield surface that the

geometry will shake down. It should be noted that all isotopically hardening materials will eventually shake down.

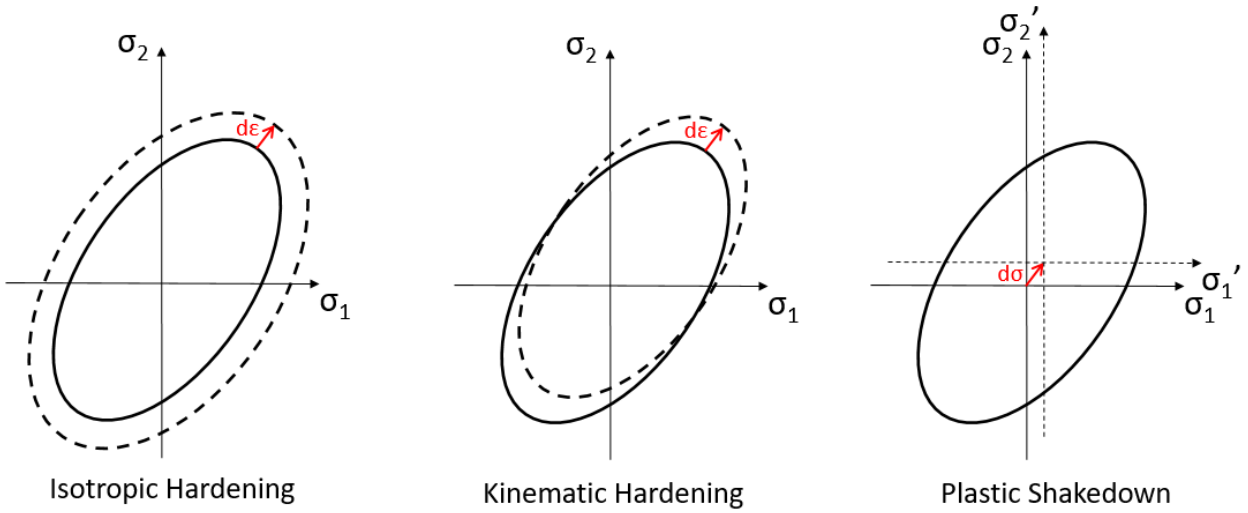


Figure 8 - Change in stress and strain fields in plasticity

Although most real materials will harden, in this project hardening will be ignored. Hardening is a material property and will therefore vary significantly dependent on the material being used. However shakedown is a phenomenon which is directly linked to the geometry and loading of a problem.

If a structure has shaken down there will be no further development of plastic strains. This is to say that we aren't deforming the material any more than it has been in the previous cycles, so it never goes out of the elastic envelope developed. This feature of a shaken down model will be used to determine in finite element analysis that the structure is fully shaken down. There is an option within Abaqus (the finite element package used) to show the residual plastic strains in a model. When this is not changing the model will be considered fully shaken down. This will also be characterised as the shape of the plastic field no longer changing with each cycle.

8 *Plastic Analysis: Defining the Variables*

The differences between the crack and incomplete contact case have been investigated using elastic analysis. The Williams' solution was used to solve analytically for the elastic stress fields. An approximate plastic zone has been calculated using elasticity and violations. However, due to the redistribution of stresses (i.e. all stresses in the plastic zone being at the yield stress and not above it) the elastic analysis will not be completely accurate; and the bigger the plastic zone the less accurate it will be. In order to get an accurate analysis an iterative approach is now implemented.

In order to approach this problem taking plasticity into consideration a finite element package will be used. Before the model can be set up calculations are required to find sensible variables to give a reasonable size plasticity zone in the model.

8.1 The Problem

We see from the analytical solution little similarity between the crack and the interface between two surfaces with infinite coefficient of friction. However, this method of analysis does not include the possibility of plastic shakedown. This is in cyclic loading where the plastic radius can change with repeated cycles. This could mean that both the crack and the interface may shakedown to the same plastic zone.

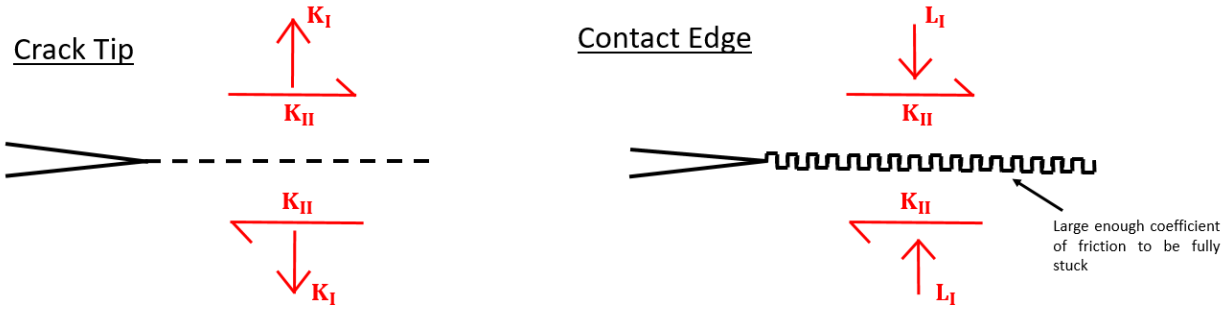


Figure 9 - An illustration of the two different geometries considered

A model will be made in Abaqus to investigate this. In this model a constant value for the symmetrical loading will be used (i.e. the L_I and the K_I) and then an oscillating fully reversing K_{II} field will be applied. A fully reversing field cannot shake down on its own, but the K_{II} field may shake down both the L_I and K_I fields leaving the two geometries with the same steady state plastic zone. A model was created using a varying displacement field. Equations for far field displacements for a crack in polar co-ordinates from Lawn and Wilshaw (4) are as follows.

Note that we are now including the customary factor of $\frac{1}{\sqrt{2\pi}}$ in the equations.

For the symmetric singular loading case when α=π:

$$\begin{pmatrix} u_{rr} \\ u_{\theta\theta} \end{pmatrix}_{K_I} = \frac{K_I}{2E}\left(\frac{r}{2\pi}\right)^{\frac{1}{2}}\begin{bmatrix} (1+\nu)\left((2\kappa-1)\cos\left(\frac{\theta}{2}\right)-\cos\left(\frac{3\theta}{2}\right)\right) \\ (1+\nu)\left(-(2\kappa+1)\sin\left(\frac{\theta}{2}\right)+\sin\left(\frac{3\theta}{2}\right)\right) \end{bmatrix} \tag{94}$$

For the antisymmetric singular loading case:

$$\begin{pmatrix} u_{rr} \\ u_{\theta\theta} \end{pmatrix}_{K_{II}} = \frac{K_{II}}{2E}\left(\frac{r}{2\pi}\right)^{\frac{1}{2}}\begin{bmatrix} (1+\nu)\left(-(2\kappa-1)\sin\left(\frac{\theta}{2}\right)+3\sin\left(\frac{3\theta}{2}\right)\right) \\ (1+\nu)\left(-(2\kappa+1)\cos\left(\frac{\theta}{2}\right)+3\cos\left(\frac{3\theta}{2}\right)\right) \end{bmatrix} \tag{95}$$

These two modes may also be linearly superimposed to give mixed mode loading.

These displacement equations from Lawn and Wilshaw (4) give the same displacement fields as those calculated from first principles in Section 2.3.

A displacement field is applied to a circular 2D surface in plain strain with a radius of 100 units. The crack is created from the centre of the circle to the left outer edge. Values of K_I and K_{II} are chosen and input into the above equations to define displacement fields applied to the computational model.

8.2 Choosing Variables

8.2.1 Crack Tip

We know from the Irwin assumption[8] that we can determine the length of the plastic zone as follows:

$$L_p = \frac{1}{\pi}\left(\frac{\Delta K_{II}}{2\tau_y}\right)^2 = \frac{3}{4\pi}\left(\frac{\Delta K_{II}}{2\sigma_y}\right)^2 \tag{96}$$

In order for the concept of small scale yielding to be valid under monotonic or cyclic loading the length of the plastic zone must be less than approximately 1/50 × the specimen dimensions.

Therefore, with a model of radius 100 units a plastic zone of around four units in length is desirable. In order to have a sensible magnitude for the yield stress we expect the stress intensity factors to be of order 1×10^9. The inputs which will be used in this model are:

$$\sigma_y = 200\text{MPa} \tag{97}$$

$$K_I = 1 \times 10^9 \text{ mm}^{1/2}\text{MPa} \tag{98}$$

$$K_{II} = 1 \times 10^9 \text{ mm}^{1/2}\text{MPa} \tag{99}$$

$$\nu = 0.3 \tag{100}$$

In plain strain

$$\kappa = 4 - 3\nu \tag{101}$$

$$E = 200\text{GPa} \tag{102}$$

$$r = 100\text{mm} \tag{103}$$

$$\mu = \frac{E}{2(1+\nu)} \tag{104}$$

$$L_p = \frac{3}{4\pi}\left(\frac{1 \times 10^3}{2 \times 2 \times 10^2}\right)^2 = 1.49\text{mm} \tag{105}$$

Model made in units of mm and MPa: *r=100, E=200000,* $K_I=1$ etcetera substituting in these variables gives the imposed displacements of:

$$\begin{pmatrix} u_{rr} \\ u_{\theta\theta} \end{pmatrix}_{K_I} = 1.296 \times 10^{-2} \begin{bmatrix} \frac{13}{5}\cos\left(\frac{\theta}{2}\right) - \cos\left(\frac{3\theta}{2}\right) \\ -\frac{23}{5}\sin\left(\frac{\theta}{2}\right) + \sin\left(\frac{3\theta}{2}\right) \end{bmatrix} \text{mm} \quad (106)$$

$$\begin{pmatrix} u_{rr} \\ u_{\theta\theta} \end{pmatrix}_{K_{II}} = 1.296 \times 10^{-2} \begin{bmatrix} -\frac{13}{5}\sin\left(\frac{\theta}{2}\right) + 3\sin\left(\frac{3\theta}{2}\right) \\ -\frac{23}{5}\cos\left(\frac{\theta}{2}\right) + 3\cos\left(\frac{3\theta}{2}\right) \end{bmatrix} \text{mm} \quad (107)$$

Stress fields for the different modes are as follows:

$$\begin{bmatrix} \sigma_{rr} \\ \sigma_{\theta\theta} \\ \sigma_{r\theta} \end{bmatrix}_{K_I} = \frac{K_I}{(2\pi r)^{\frac{1}{2}}} \begin{bmatrix} \cos\frac{\theta}{2}\left(1 + \sin^2\frac{\theta}{2}\right) \\ \cos^3\frac{\theta}{2} \\ \sin\frac{\theta}{2}\cos^2\frac{\theta}{2} \end{bmatrix} \quad (108)$$

$$\begin{bmatrix} \sigma_{rr} \\ \sigma_{\theta\theta} \\ \sigma_{r\theta} \end{bmatrix}_{K_{II}} = \frac{K_{II}}{(2\pi r)^{\frac{1}{2}}} \begin{bmatrix} \sin\frac{\theta}{2}\left(1 - 3\sin^2\frac{\theta}{2}\right) \\ \cos^3\frac{\theta}{2} \\ \sin\frac{\theta}{2}\cos^2\frac{\theta}{2} \end{bmatrix} \quad (109)$$

8.2.2 Contact Interface

For the Contact Problem we use different terms within the Williams' solution and define the coefficients for the bounded terms to be h_{ij}^{θ} terms.

$$\sigma_{ij}(r,\theta) = K_{II} r^{-\frac{1}{2}} f_{ij}^{II}(\theta) + L_I r^{\frac{1}{2}} h_{ij}^{I}(\theta) + \cdots \quad (110)$$

These coefficients have been calculated in Section 2.2.3 to be:

$$\begin{bmatrix} h_{rr} \\ h_{\theta\theta} \\ h_{r\theta} \end{bmatrix} = \begin{bmatrix} -\frac{3}{4}\cos\frac{\theta}{2} - \frac{1}{4}\cos\frac{5\theta}{2} \\ -\frac{5}{4}\cos\frac{\theta}{2} + \frac{1}{4}\cos\frac{5\theta}{2} \\ -\frac{1}{4}\sin\frac{\theta}{2} + \frac{1}{4}\sin\frac{5\theta}{2} \end{bmatrix} \quad (111)$$

This gives rise to the stress vector below for the square root bounded mode I stresses.

$$\begin{bmatrix} \sigma_{rr} \\ \sigma_{\theta\theta} \\ \sigma_{r\theta} \end{bmatrix} = L_I \left(\frac{r}{2\pi}\right)^{\frac{1}{2}} \begin{Bmatrix} -\frac{3}{4}\cos\frac{\theta}{2} - \frac{1}{4}\cos\frac{5\theta}{2} \\ -\frac{5}{4}\cos\frac{\theta}{2} + \frac{1}{4}\cos\frac{5\theta}{2} \\ -\frac{1}{4}\sin\frac{\theta}{2} + \frac{1}{4}\sin\frac{5\theta}{2} \end{Bmatrix} \quad (112)$$

As calculated in Section 2.3.1 the displacements are:

$$\begin{bmatrix} u_{rr} \\ u_{\theta\theta} \end{bmatrix}_{L_I}^{S} = \frac{r^{\frac{3}{2}} L_I}{12\mu} \begin{bmatrix} -\cos\frac{5\theta}{2} + (2\kappa - 3)\cos\frac{\theta}{2} \\ 5\sin\frac{5\theta}{2} + (2\kappa + 3)\sin\frac{\theta}{2} \end{bmatrix}$$

The variables defined in Section 8.2.1 are also used here. The value of L_I to be used is calculated later on when it comes to applying these displacements to my computational model.

8.3 *Finding the Plastic Radii*

The expected size of the plastic radius for a yield stress of 200MPa will be calculated at various points around the yield surface so that the Abaqus model may be checked against the known analytical solution. This will be calculated using the purely elastic case with the individual modes before turning on plasticity and combining modes.

These plastic radii are calculated with the normalised stress vectors in Lawn and Wilshaw (4).

8.3.1 Mode I

From Section 2.4 on the line $\boldsymbol{\theta = \theta}$ we have

$$\sigma_y = \frac{K_I}{(2\pi r_p)^{\frac{1}{2}}} 0.4\text{MPa} \tag{113}$$

If $\sigma_y = 200MPa$ then

$$r_p = \left(\frac{0.4K_I}{\sigma_y}\right)^2 \frac{1}{2\pi} = \left(\frac{0.4 \times 1 \times 10^9}{2 \times 10^8}\right)^2 \frac{1}{2\pi} = 0.636\text{mm} \tag{114}$$

$$\sigma_y \frac{(2\pi r_p)^{\frac{1}{2}}}{K_I} = \frac{1}{\sqrt{2}}\left[\left(\frac{3\sqrt{2}}{4} - \frac{\sqrt{2}}{4}\right)^2 + \left(\frac{\sqrt{2}}{4} - \frac{3\sqrt{2}}{10}\right)^2 + \left(\frac{3\sqrt{2}}{10} - \frac{3\sqrt{2}}{4}\right)^2 + 6\left(\frac{\sqrt{2}}{4}\right)^2\right]^{\frac{1}{2}} \tag{115}$$

$$= 0.911$$

Now we calculate the plastic radius for the line $\theta = \frac{\pi}{2}$ using equations from Section 2.4.

$$\sigma_y = \frac{K_I}{(2\pi r_p)^{\frac{1}{2}}} 0.911 \tag{116}$$

Therefore to find the plastic radius for mode 1 loading at an angle of $\theta = \frac{\pi}{2}$ from a rearrangement of the above with $\sigma_y = 200MPa$:

$$r_p = \left(0.911\frac{K_I}{\sigma_y}\right)^2 \frac{1}{2\pi} = \left(0.911\frac{1 \times 10^9}{2 \times 10^8}\right)^2 \frac{1}{2\pi} = 3.302\text{mm} \tag{117}$$

Table 2 - Plastic Radii for Mode I

Angle (radians)	Plastic Radius r_p (mm)

0	0.636
$\frac{\boldsymbol{\pi}}{\mathbf{2}}$	3.302

8.3.2 Mode II

From Section 2.4 on the line $\theta = 0$ we have

$$\sigma_y = \frac{K_{II}}{(2\pi r)^{\frac{1}{2}}} 1.73 \tag{118}$$

If σ_y = 200MPa then

$$r_p = \left(1.73 \frac{K_{II}}{\sigma_y}\right)^2 \frac{1}{2\pi} = \left(1.73 \frac{1 \times 10^9}{200 \times 10^6}\right)^2 \frac{1}{2\pi} = 11.9\text{mm} \tag{119}$$

On the line $\theta = \frac{\boldsymbol{\pi}}{\mathbf{2}}$ gives

$$\sigma_y = \frac{K_{II}}{(2\pi r)^{\frac{1}{2}}} 0.911 \tag{120}$$

If σ_y = 200MPa then

$$r_p = \left(0.911 \frac{K_{II}}{\sigma_y}\right)^2 \frac{1}{2\pi} = \left(0.911 \frac{1 \times 10^9}{200 \times 10^6}\right)^2 \frac{1}{2\pi} = 3.302\text{mm} \tag{121}$$

Table 3 - Plastic Radii for Mode II

Angle (radians)	**Plastic Radius r_p (mm)**

0	11.9
$\boldsymbol{\frac{\pi}{2}}$	3.302

The yield stress to be used in the finite element model is also 200MPa, therefore these values may be used for direct comparison.

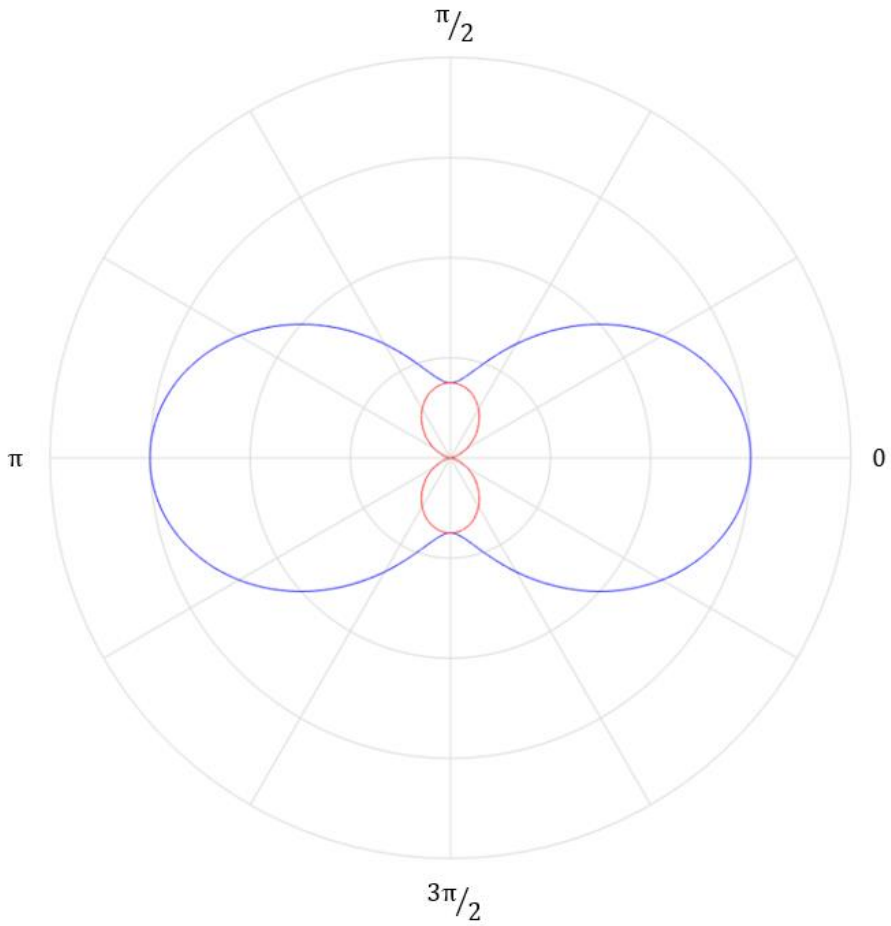


Figure 10 - Graph of K_I and K_{II} plastic radii created in MATLAB

9 *Plastic Analysis: Simplifying Assumptions for FEA*

In the model to be created in Abaqus several simplifying assumptions have been made. This is for ease of analysis; to make it less computationally 'expensive' to get the desired result. The three assumptions made are detailed below.

9.1 Displacement vs Load Control

It is computationally easier to do displacement control for modelling in Abaqus as it automatically prevents any free body movement. It will give the same result for the first loading cycle but in the second and following cycles the load applied will be slightly greater than that applied in the first cycle because of the residual displacements caused by yielding of elements.

A considerable amount of time was lost on the project with little progress due to an apparent complete lack of any shakedown behavior. It was discovered that this subtle difference is very important. This was then tried here and it became evident that shakedown will only occur if the displacements imposed on the model are a little less than those originally exerted. This will ensure we are never subjecting the model to a load *greater than or exactly equal to* that in the first cycle. If we think in terms of the axes of the yield surface moving this makes sense as otherwise due to slight overloading the load cycle can never become purely elastic as it always slightly exceeds the previous stress and therefore the yield surface.

Thus, only 95% of the total displacement was subsequently used in the second and following cycles. This ensures that the stress does not exceed that of the first cycle and, as we can see in Section 11.3 onwards allows for shakedown behavior to occur.

9.2 The Use of a Keyhole at the Crack Tip

The crack tip, or contact edge generates a singularity. This causes an infinite stress at the apex and hence very large strains. This is very hard to solve numerically and computationally expensive for the finite element package to compute. Therefore, a small 'hole' is made in the model at the crack tip.

This, obviously, introduces a slight inaccuracy and a dimension in an otherwise dimensionless problem. However, we can show how insignificant this slight geometrical change is by comparing a model with and without the hole. In addition it can also be shown that if the loads are changed slightly (and therefore the ratio of the hole to the plastic zone changes) that there is no difference in their inaccuracies. The hole used in this model has a radius of 0.01units and the total model is 100 units. This allows for the plasticity zone being less than $1/50^{th}$ of the size of the total model and then the hole being less than $1/50^{th}$ the size of the plastic zone. Small scale yielding assumptions may therefore be applied.

9.3 Setting Displacements to zero rather than releasing them

It was originally thought that a given displacement would be applied to the model and then released to allow the model to return to a zero stress state. It should be noted that this is different from modifying a set boundary condition to have zero magnitude. If the model were still in the elastic regime they would be one and the same but this is not the case with this model. Whenever we go into the plastic regime irreversible distortion of elements will occur. This means that by returning to a zero displacement state we are not in fact returning to a zero stress state, but instead applying a stress in the opposite direction to the original load/displacement.

However, if the plastic zone is very small in relation to the total model, where the boundary conditions are being applied at the edges then it can be shown that applying a zero displacement and a zero stress condition are effectively the same thing.

10 *Plastic Analysis: Creating the Finite Element Model*

10.1 Creating the Geometry

The finite element analysis software Abaqus was used to create the model to be used to determine the similarities of a crack tip and contact interface in this project. In the first instance an elastic model was used to verify the shape and size of the plastic zone was as expected, then plasticity was introduced and used to compare the steady state plasticity zones of the two geometries.

The model was made with the geometry shown in Figure 11 below. A circular model is used as polar displacement fields are to be applied. It is made of a solid homogenous material of yield strength 200MPa and Poissons ration 0.3.

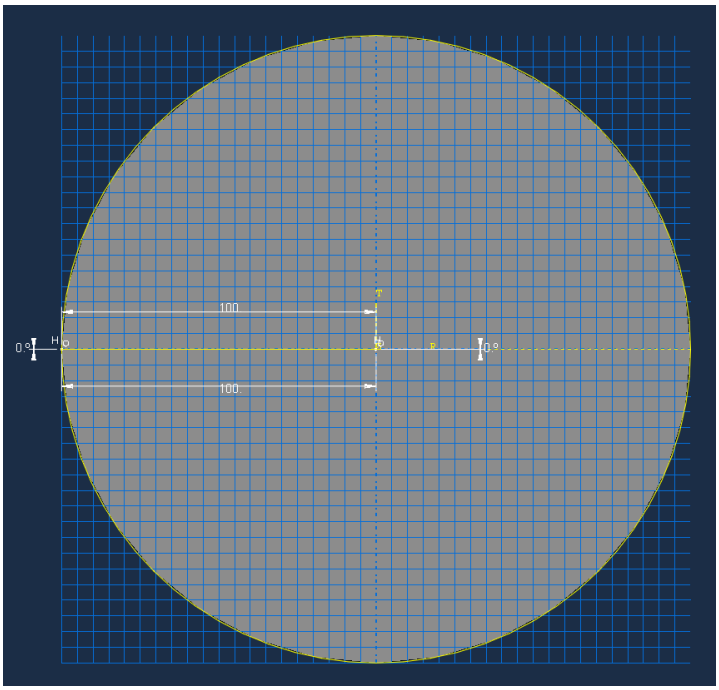


Figure 11 - The geometry drawn in Abaqus

As discussed in Section 9 there is a small keyhole at the apex of the crack. This keyhole is present as otherwise the singularity at the apex of the crack makes the finite element analysis far harder to compute. The keyhole is only 0.01 units in radius and therefore will not make a difference to the overall stress field.

Then onto this surface a sketch was created to enable finer mesh closer to the apex of the crack tip or interface. The total radius of the model was 100 units then there are contours at 5 units, 1 unit and 0.01 units.

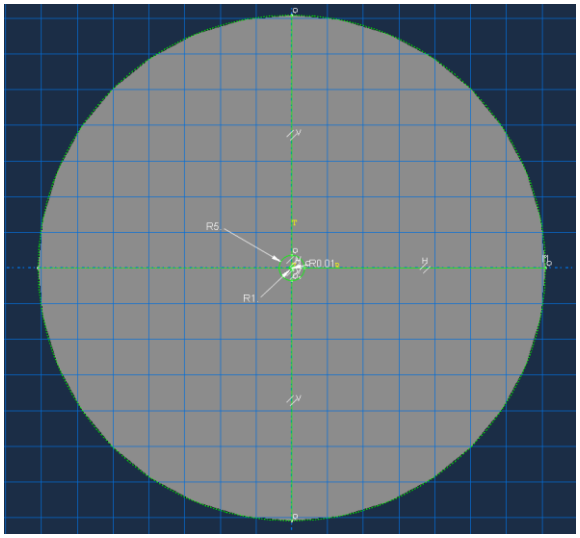


Figure 12- The sketch used to create the mesh in my Abaqus model

The mesh was then created. The outer elements are 5 units, at the 5 unit contour they are 0.25 units, at the 1 unit contour they are 0.05 units and at the 0.01 units contour they are 0.0001 units, they are all 0.0001 units at any r value less than 0.01. The seeding used was uniform around the contours and single bias on the spokes between contours to linearly reduce the element size. Standard Linear Elements in Quad Dominated Element Shape were then used in a Sweep Mesh. As is shown in Figure 13 below.

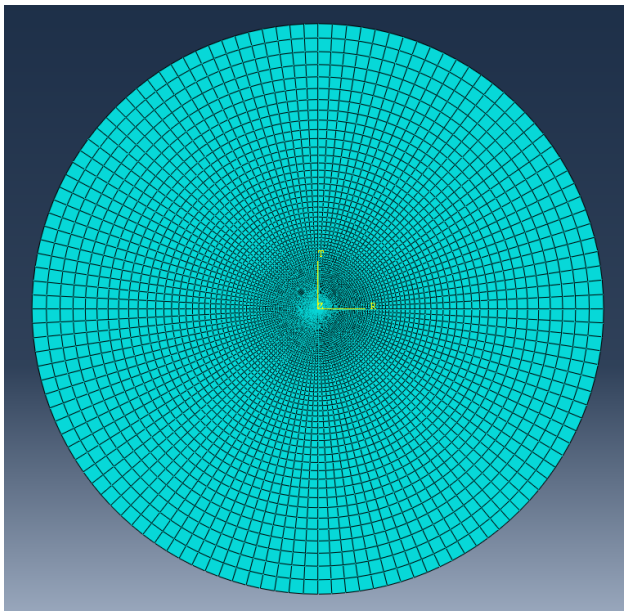


Figure 13 - The sweep mesh used

10.2 Applying the Displacements

The displacement fields (as detailed in Section 0) were applied in polar co-ordinates on the edge of the model. Displacement fields were favored over stress fields as they will ensure there is no free body movement of the model. Analytical fields in terms of r and θ were input into Abaqus.

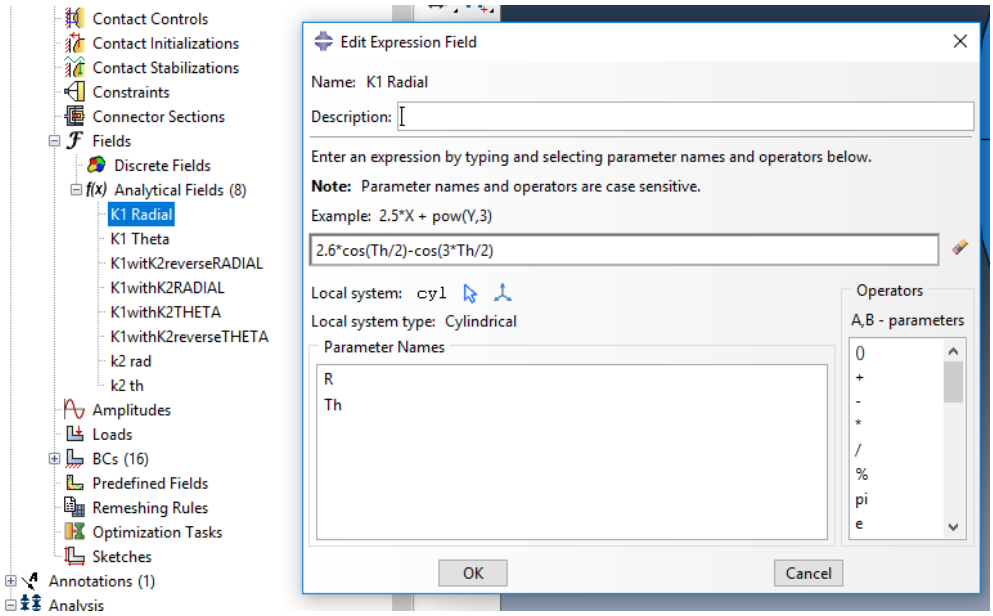


Figure 14 - Detail of defining an analytical field in abaqus

Then these were applied to the boundaries of the model in the required steps as boundary conditions. As shown in Figure 15 below, the amplitudes applied are as calculated in the previous section of this thesis.

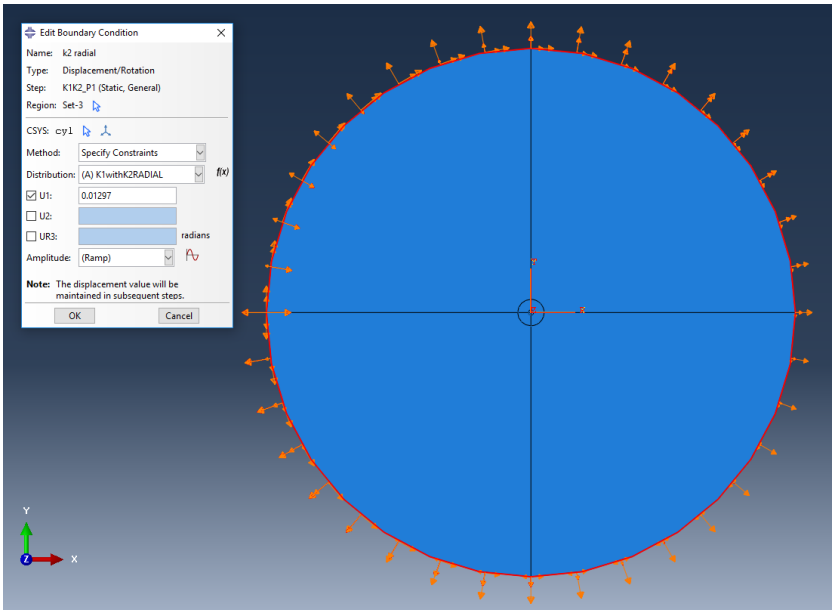


Figure 15 - Analytical Fields being applied in a polar co-ordinate set to give the desired stress field

11 *Plastic Analysis: Results from Finite Element Analysis*

This section details the main output of this thesis. It shows the way in which the results were obtained to demonstrate that an incomplete contact and crack tip do exhibit the same behavior when subjected to the relevant mode 1 loading and an oscillatory mode 2 loading.

11.1 Comparison to Elasticity Model

Firstly, the Elastic Model was made and the size and shape of it is verified by checking it against the analytical model. This ensured the correct boundary conditions were being applied.

Mode I

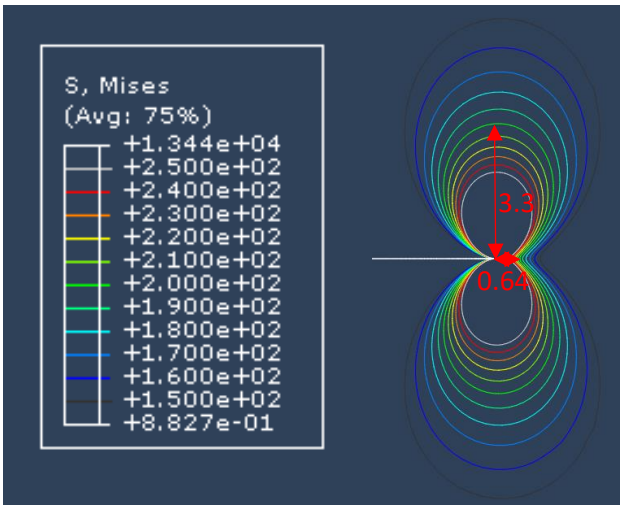


Figure 16 - Symmetric Mode I Elastic Stress Field. Yield stress = 200(MPa)

Mode II

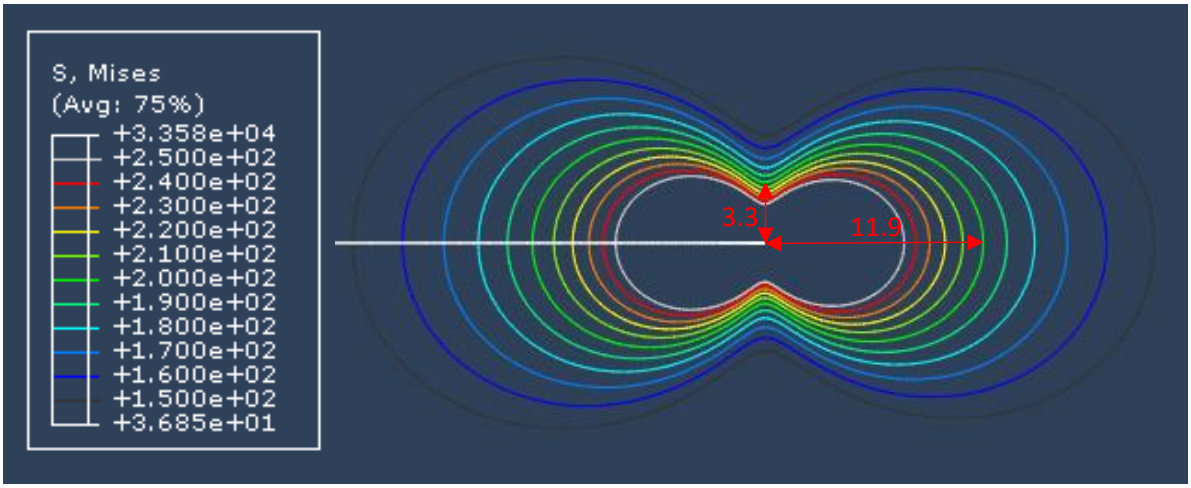


Figure 17 - Singular Mode II Elastic Stress Field. Yield stress =200(MPa)

It can be seen for both mode I and mode II that the size of the plain strain plastic zones using elasticity and violations is the same at that calculated in Section 2.4. This verifies that the model is correct.

Then plasticity is turned on, this will mean there is a plastic zone at the crack tip and that deformation will occur there. This will cause inaccuracies in using the displacement approach rather than the stress approach.

11.2 Introducing Plasticity

When plasticity is turned on the stress fields will change. This is because when we are in purely elastic analysis it is assumed that stresses may occur at values higher than that of yield. When plasticity is introduced stress is capped at yield stress (200MPa here). Therefore the redistribution of stresses will cause a different shape and a larger plasticity field. These new fields can be seen in the figures below.

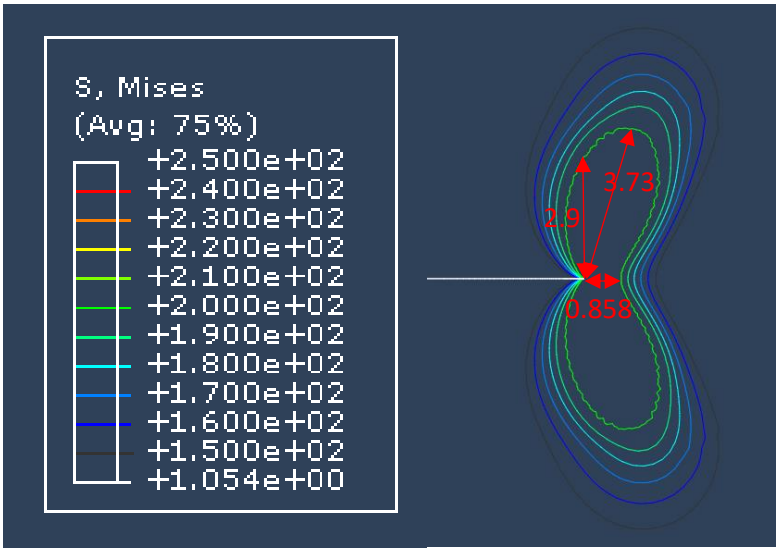


Figure 18 - K_I stress field with plasticity

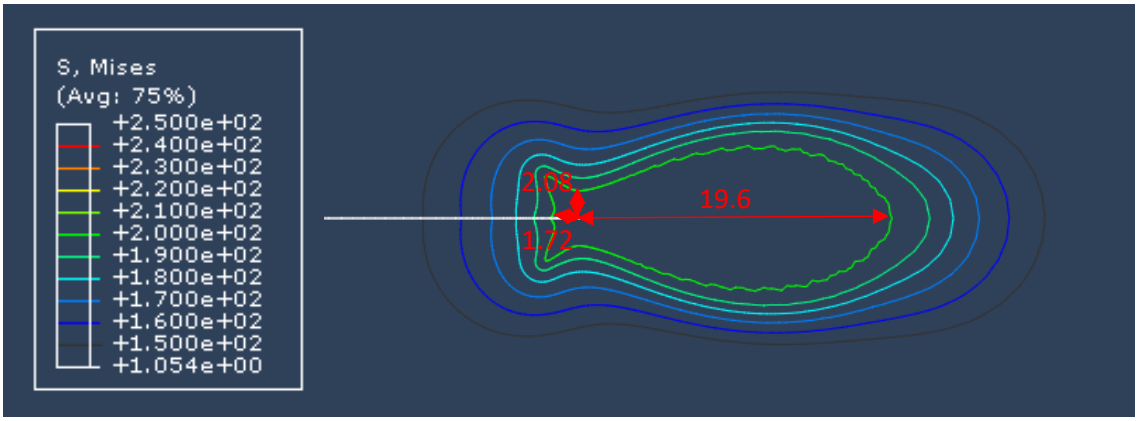


Figure 19 - K_{II} stress field with plasticity

We can see how the mode I and mode II stress fields change due to the redistribution of the stresses in plastic analysis. Also note that the stress now never exceeds the set yield stress of 200MPa.

It can be seen here that the plastic zone in mode II has a plastic radius of approximately $1/5^{th}$ of the total model size. This is too large to still consider small scale yielding. We want a plastic zone much smaller than this. Therefore the yield stress used is changed, a yield stress of 50MPa is used from this point onwards.

11.3 Loading in One Direction

Firstly, the displacement field is applied in just the positive direction, it is oscillated between positive and zero repeatedly until a steady state is reached. It can be seen that the residual stress field when no displacement is applied is smaller and opposite in sign to the original stress field. The point of this oscillation is that it should be seen that both the K_{II} and K_I fields can shake their own stress field down if loaded in a single direction.

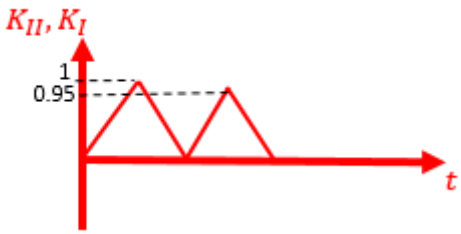


Figure 20 - Loading Cycle

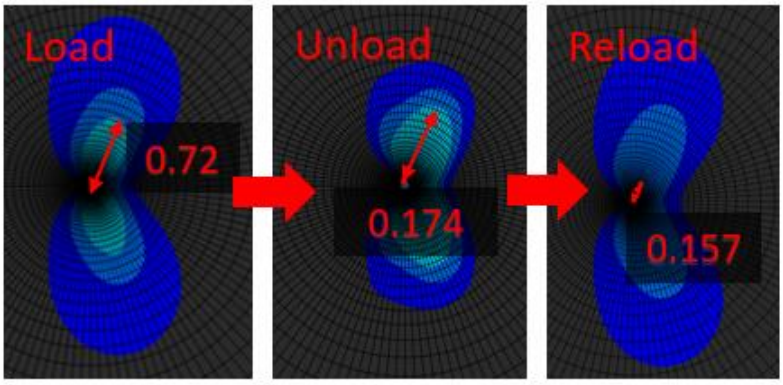


Figure 21 - K_I Stress Field. Left to right; load, unload, reload.

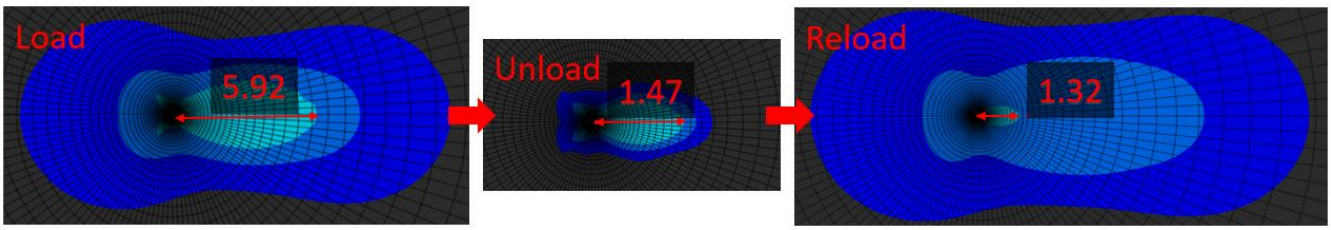


Figure 22 - Stress Fields for Loading in K_{II}

In Figure 22 it can be seen that the K_{II} field shakes its own plasticity zone down. That is that in the reload cycle the plasticity zone (indicated by the lightest blue and the red arrows) is approximately $\frac{2}{9}ths$ of the original plasticity zone. Theoretically the expected size of the reverse cyclic damage is expected to be ¼ of the size of the plasticity zone.[9]

11.4 Positive and Negative Loading

For the full analysis of the crack tip we must look at what happens when we load with a K_I stress field and then oscillate the K_{II} field. Firstly we will find the K_{II} field when we oscillate the direction of loading for solely antisymmetric (K_{II}) loading. Here we expect no shakedown as shakedown cannot occur if the direction of loading is changing.

Figure 23 shows the K_{II} loading used, it should be noted that the stress concentration factor K_{II} has been normalised in this figure. In the first positive loading cycle we take K_{II} to be $5x10^8$ $[FL^{-3/2}]$ and we load to full displacement. In the first negative loading cycle and following positive and negative loading we only load to 95% of the displacement to ensure the displacement is less than initial and therefore shakedown will occur, if possible.

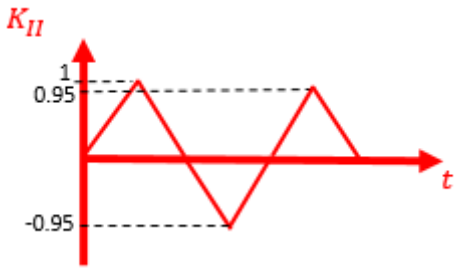


Figure 23 - The K_{II} loading (1.5 cycles shown)

In this analysis we measure the plastic zone in two ways. Firstly, by measurement of the value of the plastic radius at zero degrees, as defined in the Williams' solution. And secondly by looking at the physical shape of the plastic zone outputted from the Abaqus analysis and comparing them for different loading cases and in different cycles.

Table 4 shows the relative size of the plasticity zone in each loading step. The key below shows the colours used to depict different stresses on the Abaqus output. It should be noted that as the model is elastic perfectly plastic (i.e. no hardening) there will be no stresses present above the yield stress;

which is now 50MPa. It should also be noted that Figure 25 is not to scale, as the unloading phase is approximately ¼ of the size of the loading. The image is rescaled to emphasise the shape of the plastic zone in different steps.

Table 4 - The development of the plastic field for oscillating K_{II} loading

Step name	Direction of Loading	Plastic Radius at Zero Degrees	Change from Previous Cycle
Load 1	+	5.72	N/A
Unload 1	0	1.44	N/A
Load 2	-	5.24	-0.47
Unload 2	0	1.31	-0.12
Load 3	+	5.24	0
Unload 3	0	1.31	0
Load 4	-	5.24	0
Unload 4	0	1.31	0
Load 5	+	5.24	0
Unload 5	0	1.31	0
Load 6	-	5.24	0
Unload 6	0	1.31	0

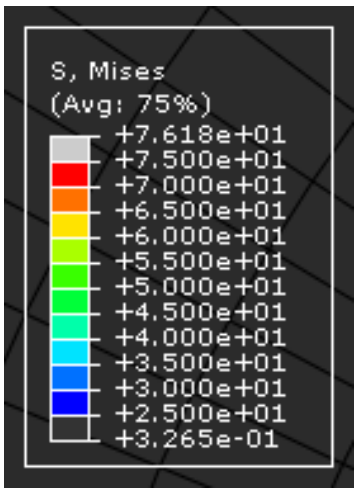


Figure 24 - Key for Stress Fields in Figure 25 and Figure 27.

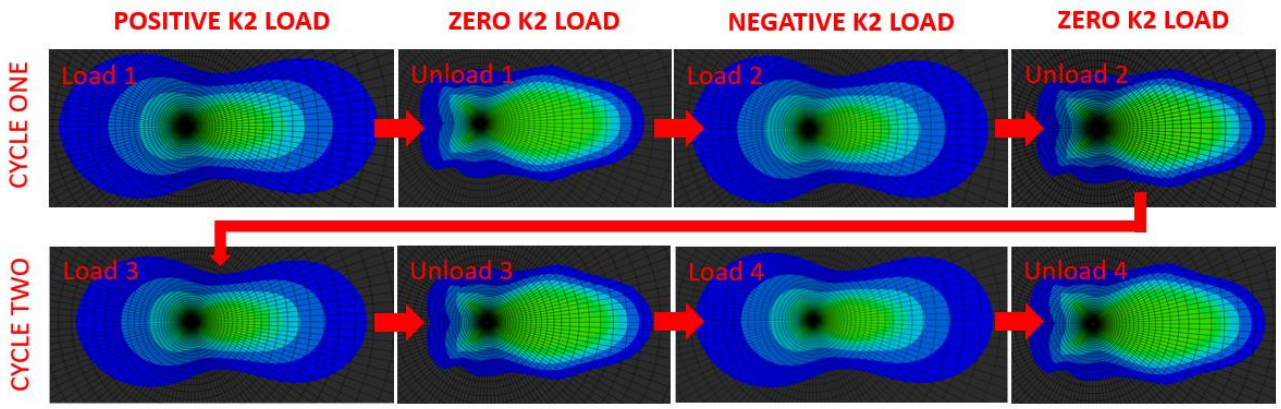


Figure 25 - The stress field output for cyclically loading K_{II} (not to scale)

It can be seen that the remaining plastic field after *unloading* is almost exactly ¼ of the loaded plastic zone size. It is also confirmed that when the K_{II} load is re-applied there is no shakedown, i.e. the plastic zone is of the same size and shape as that experienced on initial loading. The same is true in cycle two.

We now preload the model with a K_I stress field, and hold constant, before applying the oscillating K_{II} field. What we expect is that the plasticity zone will become, in the steady state, very similar to that in the case above. The K_{II} represents the shear load which, as in reality it is limited by friction, we expect to be very approximately half of the normal load if the coefficient of friction were say, about 0.8, which is a realistic figure. Therefore the K_I load applied is double that of K_{II}, so $K_I = 1 \times 10^9$ $FL^{-3/2}$ *and* $K_{II} = 5 \times 10^8$ $FL^{-3/2}$.

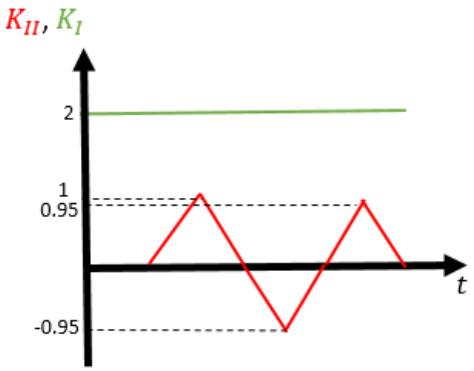


Figure 26 - K_I loading held constant as K_{II} is oscillated at half its' value

Table 5 - The development of the plastic field for constant K_I and oscillating K_{II} loading

Step	Direction of Loading	Plastic Radius at Zero Degrees	Change from Previous Cycle
K_I LOAD	+	2.88*	N/A
Load 1	+	5.87	N/A
Unload	0	1.51	N/A
Load 2	-	5.45	N/A
Unload 2	0	1.37	-0.14
Load 3	+	5.33	-0.54
Unload 3	0	1.33	-0.04
Load 4	-	5.33	-0.12
Unload 4	0	1.33	0
Load 5	+	5.33	0
Unload 5	0	1.33	0
Load 6	-	5.33	0
Unload 6	0	1.33	0

*this is the maximum plastic radii for the K_I case, not the value along the line $\theta = 0$

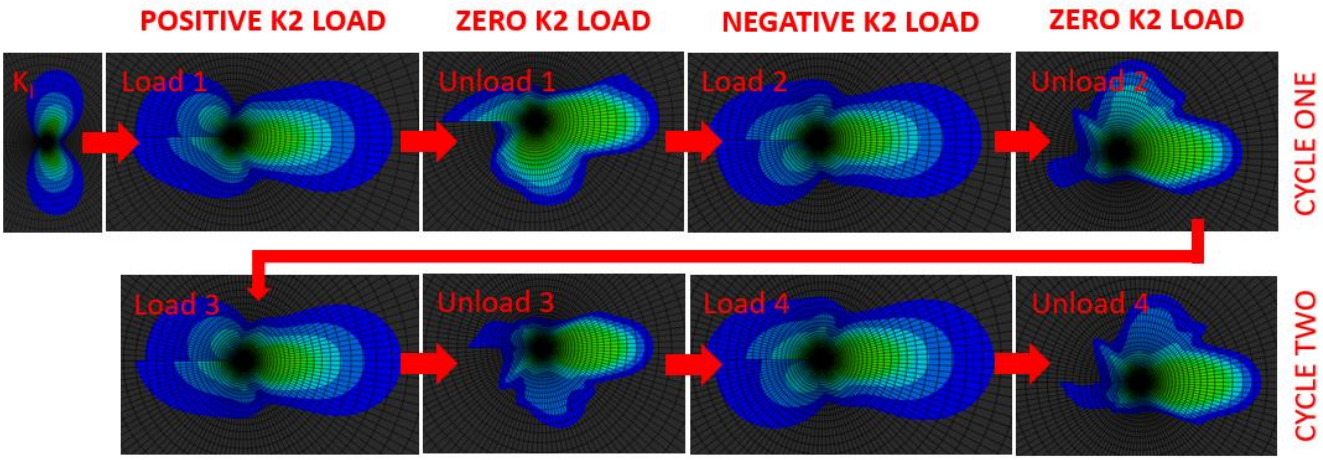


Figure 27 – Constant K_I pressure load with oscillating K_{II} shear load (not to scale)

Again, here it should be noted that the images in Figure 27 are rescaled to emphasise the shape of the plastic zone and that the relative sizes of the stress fields can be found in Table 5.

Table 6 - Comparison of Different Loading Cycles

Step	K_{II} alone	K_I plus K_{II}	Percentage Difference (%)
Load 1	5.72	5.87	2.6
Unload 1	1.44	1.51	4.9
Load 6	5.24	5.33	1.7
Unload 6	1.31	1.33	1.5

It can be seen from these results that the K_I and K_{II} combined loading shakes down to a stress field very similar to the purely K_{II} loading. That is that the oscillating K_{II} load shakes down the K_I load, but there is no shakedown effect on the K_{II} load. The difference in the size of the residual stress field is a difference of +1.5% and for the fully loaded part of the cycle a difference of +1.7% is seen. Compared to the difference in the first cycle we can see that, as the stress field shakes down it becomes far more similar to that for the K_{II} oscillatory loading. In addition there is some inaccuracy in the method of measurement as there are finite nodes to measure from rather than a continuous scale. It should be noted that the same effect of shakedown of the K_I field is seen if we load the K_{II} to the same displacement each time. It is only required that the stress is decreased for the K_{II} to shakedown itself and not other fields. The results which are shown with 100% in the first load and 95% thereafter to allow for comparison to other loading scenarios.

11.5 Contact Edge

The contact edge problem will be more difficult to solve than the crack tip as there is a larger area of plasticity. Ideally, we want the edge of the model to *just* be going into plasticity when the normal load is applied or, indeed, to be below the yield condition. We certainly would not expect wholescale plasticity to be present when the normal load, alone, is applied.

***11.5.1** Attachment to an Example Problem*

In order to analyse the contact edge and select a sensible ratio of $\frac{K_{II}}{L_I}$ we must consider how it could be applied to different geometries. I will be considering its application to a Hertzian contact and using this to find a sensible ratio to use for the two stress intensity factors.

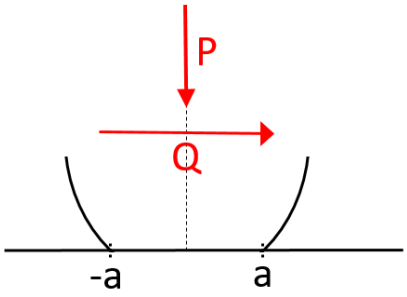


Figure 28- A Hertzian Contact Probelem

The variable *a* here represents the half-width of the hertzian contact. The following equations can be found in a paper on partial slip in incomplete contacts[10].

$$K_{II} = \frac{Q}{\pi\sqrt{2a}} \tag{122}$$

$$L_I = \frac{1}{\pi}\sqrt{\frac{2}{a}} = \frac{dP}{da} \tag{123}$$

For a Hertzian contact

$$L_I = \frac{1}{\pi}\sqrt{\frac{2}{a}} = \frac{dP}{da} = \frac{P}{\pi}\sqrt{\frac{8}{a^3}} \tag{124}$$

Therefore we can calculate the ratio between K_{II} and L_I which is realistic to represent the Hertzian contact.

$$\frac{K_{II}}{L_I} = \frac{Q}{\pi\sqrt{2a}}\frac{\pi}{P}\sqrt{\frac{a^3}{8}} = \frac{Qa}{4P} \tag{125}$$

We know from Colombs's law of friction that in order for no slip to occur, where *f* is the coefficient of friction.

$$Q < fP \tag{126}$$

If we take the coefficient of friction to be 0.5 then

$$\frac{K_{II}}{L_I} = \frac{a}{8} \tag{127}$$

We know from the Williams' Solution that

$$\sigma_{rr}^{K_{II}} = \frac{K_{II}}{\sqrt{r_0}} f_{rr}^{II}(\theta) \tag{128}$$

$$\sigma_{rr}^{L_I} = L_I \sqrt{r_0} h_{rr}^{I}(\theta) \tag{129}$$

$$\frac{\sigma_{rr}^{K_{II}}}{\sigma_{rr}^{L_I}} = \frac{K_{II}}{L_I} \frac{1}{r_0} \frac{f_{rr}^{II}(\theta)}{h_{rr}^{I}(\theta)} = \frac{a}{r_0} \frac{1}{8} \frac{f_{rr}^{II}(\theta)}{h_{rr}^{I}(\theta)} \tag{130}$$

Where r_0 is the radius of the model created in Abaqus.

Now, in order to define the sizes of the stresses the ratio between *a* and r_0 needs to be determined. If we look at Figure 28 we can see that the maximal value r_0 can have is *a*. As if r_0 exceeds *a* then the effects of the other edge of the contact will be prevalent. As the geometry is symmetrical we would expect a symmetrical stress field.

$$r_0 \leq a \tag{131}$$

$$\frac{K_{II}}{L_I} \leq \frac{1}{8}[\mathrm{L}] \tag{132}$$

Different ratios of $\frac{K_{II}}{L_I}$ can be used within this range.

11.5.2 Modelling

The same value of K_{II} will be used as was used in the crack tip interface for consistency. The magnitude of the K_{II} load will also be reduced by 5% after the first load, as in the other two cases. Therefore the initial values of the stress intensity factors to be used are.

$$K_{II} = 5 \times 10^8\ [\mathrm{FL}^{-3/2}] \tag{133}$$

$$(L_I)_{max} = 4 \times 10^9\ [\mathrm{FL}^{-5/2}] \tag{134}$$

From earlier calculations we know that.

$$\begin{bmatrix} u_{rr} \\ u_{\theta\theta} \end{bmatrix}_{L_I}^{S} = \frac{5r^{\frac{3}{2}}L_I}{8\mu} \begin{bmatrix} -\cos\frac{5\theta}{2} + (2\kappa - 3)\cos\frac{\theta}{2} \\ 5\sin\frac{5\theta}{2} + (2\kappa + 3)\sin\frac{\theta}{2} \end{bmatrix} \tag{135}$$

Substitute in *r=0.1, E=200*GPa, *v=0.3*

$$\mu = \frac{E}{2(1+\nu)} = \frac{50 \times 10^9}{2.6} = 1.92 \times 10^4 \mathrm{MPa} \tag{136}$$

$$\begin{bmatrix} u_{rr} \\ u_{\theta\theta} \end{bmatrix}_{L_I}^{S} = \frac{5r^{\frac{3}{2}} \times L_I}{8 \times 1.92 \times 10^{10}} \begin{bmatrix} -\cos\frac{5\theta}{2} + 0.6\cos\frac{\theta}{2} \\ 5\sin\frac{5\theta}{2} + 6.6\sin\frac{\theta}{2} \end{bmatrix} = 10.28 \times 10^{-13} L_I \begin{bmatrix} -\cos\frac{5\theta}{2} + 0.6\cos\frac{\theta}{2} \\ 5\sin\frac{5\theta}{2} + 6.6\sin\frac{\theta}{2} \end{bmatrix} \tag{137}$$

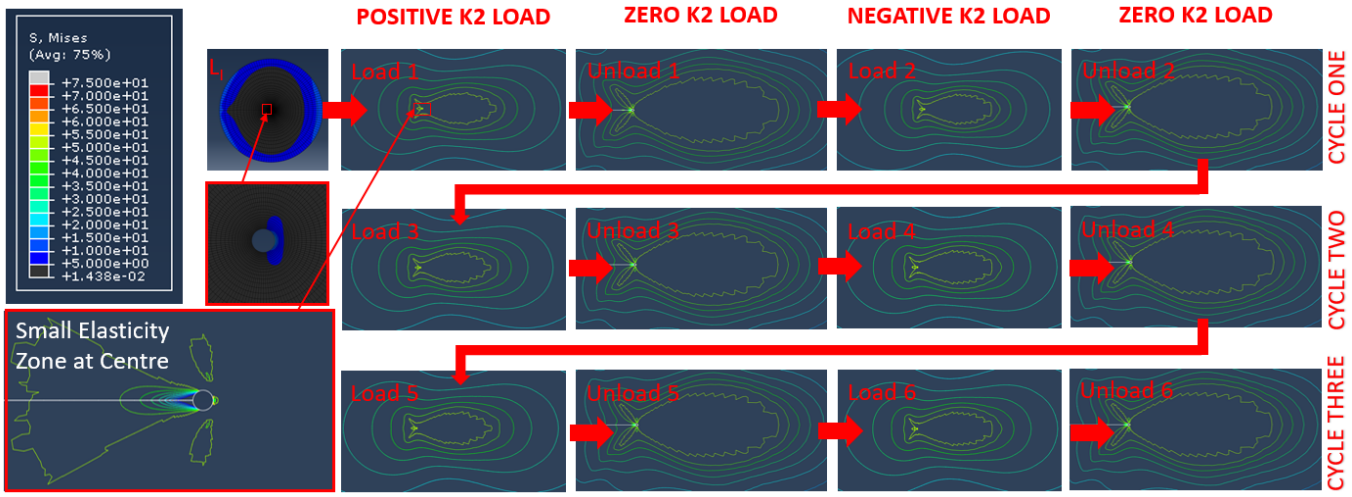
Using the maximum possible length where r_0 (the radius of my model) is equal to a (the half length of a Hertzian contact).

$$L_I = 4 \times 10^9 [\mathrm{FL}^{-5/2}] \tag{138}$$

$$\begin{bmatrix} u_{rr} \\ u_{\theta\theta} \end{bmatrix}_{L_I}^{S} = 10.28 \times 10^{-13} L_I \begin{bmatrix} -\cos\frac{5\theta}{2} + 0.6\cos\frac{\theta}{2} \\ 5\sin\frac{5\theta}{2} + 6.6\sin\frac{\theta}{2} \end{bmatrix} = 0.004112 \begin{bmatrix} -\cos\frac{5\theta}{2} + 0.6\cos\frac{\theta}{2} \\ 5\sin\frac{5\theta}{2} + 6.6\sin\frac{\theta}{2} \end{bmatrix} \tag{139}$$

Table 7 - Stress Fields for the Incomplete Contact

Step	Direction of Load-ing	Start of Plastic Zone		End of Plastic Zone (A)	Change Since Previous Cycle		
		Left of Hole (L)	Right of Hole (R)		L	R	A
L1 Load		>100	0				
Load 1	+	0.165	0.00472	5.72			
Unload 1	0	N/A	0.00472	1.44			
Load 2	-	0.165	0.00472	5.24	0	0	-0.58
Unload 2	0	N/A	0.00472	1.31	0	0	-0.14
Load 3	+	0.165	0.00472	5.24	0	0	0
Unload 3	0	N/A	0.00472	1.31	0	0	0
Load 4	-	0.165	0.00472	5.24	0	0	0
Unload 4	0	N/A	0.00472	1.31	0	0	0
Load 5	+	0.165	0.00472	5.24	0	0	0
Unload 5	0	N/A	0.00472	1.31	0	0	0
Load 6	-	0.165	0.00472	5.24	0	0	0
Unload 6	0	N/A	0.00472	1.31	0	0	0



Several things are worth noting from these results. There is a small zone of plasticity at the right hand side of the contact edge where the stress increases in the initial L_I loading case. This will be due to small inaccuracies within the finite element model and is not part of the field defined by the purely square root bounded solution – it is because tiny amounts of other eigensolutions, including the (unwanted) singular term, are probably present. Once the singular mode II field is applied this swamps the problem and dominates the solution. But with the noticeable exception that there is a small central zone of elasticity to the left and right of the contact edge. It was not initially clear whether this small zone of elasticity is present due to the L_I field itself or the inaccuracies introduced by adding it. However, on closer inspection of the earlier K_{II} loading case (on its own) it can be seen that there is also a small elasticity zone of the same size and shape present. This indicated that this small elasticity zone is simply a function of inaccuracies in the method of computation, i.e. the finite element package.

Various different values of L_I could be investigated but it is apparent that this is not necessary. If the largest possible L_I value is shaken down then any smaller field will be too.

Table 8 - A comparison of the plastic radii

Step	**K_{II} alone**	**K_I plus K_{II}**	**Percentage Difference (%)**	**L_I plus K_{II}**
Load 1	5.72	5.87	2.6	5.72
Unload	1.44	1.51	4.9	1.44
Load 6	5.24	5.33	1.7	5.24
Unload 6	1.31	1.33	1.5	1.31

It can be seen in Table 8 that the values obtained for the L_I plus K_{II} field are exactly the same as the K_{II} loading alone. It should also be noted that the plastic radii in the K_I plus K_{II} case could be closer in value to the other two than seen here. The measurements were taken by looking at the contours in Abaqus and as such there is a reasonable error in both reading the measurements and due to slight inaccuracies in the modelling. An analysis with a finer mesh at the areas of interest would be needed

for higher levels of accuracy. However, it is obvious from the readings and the shape of the plasticity zone shown in the results (see Figure 26) that the K_I stress field does have a far more disruptive effect on the central stress field, as expected. The influence of the K_I at the centre was far larger than that of the L_I and therefore more shakedown action was required – as can be seen by the initial values in Table 8.

No further L_I values will be examined. The case looked at in detail was the maximum ratio of $\frac{K_{II}}{L_I}$ and therefore any other valid value of L_I will be lower and thus just decrease the effect of the L_I field. As it is seen that the L_I has minimal effect when at its maximal value we can therefore conclude it will always have a minimal effect.

The results from the computational analysis may be normalised with reference to the size of the K_{II} field calculated through analytical analysis. For the final simulations the following variables were used:

$$\sigma_y = 50MPa \tag{140}$$

$$K_I = 1 \times 10^9 \text{ mm}^{1/2}\text{MPa} \tag{141}$$

$$L_I = 4 \times 10^9 \text{ mm}^{-1/2}\text{MPa} \tag{142}$$

$$K_{II} = 5 \times 10^8 \text{ mm}^{1/2}\text{MPa} \tag{143}$$

$$\nu = 0.3 \tag{144}$$

$$\kappa = 4 - 3\nu \tag{145}$$

$$E = 50\text{GPa} \tag{146}$$

$$r = 100\text{mm} \tag{147}$$

11.6 Verification of No Slip Edge Condition

It is seen that when the L_I stress field and K_{II} stress field are combined that to the right of the model, where the contact interface is, there is a large plasticity zone. This zone is, at its smallest 1.31 units in length along the interface.

If we look at Figure 5 from earlier in this report (the same as Figure 29 here) then we can see the zone of frictional slip will change dependant on the coefficient of friction for any given Q/P ratio. Throughout this project a Q/P ratio of 0.5 is used. Therefore any coefficient of friction which is higher than 0.5 will mean there is a stuck portion of the contact.

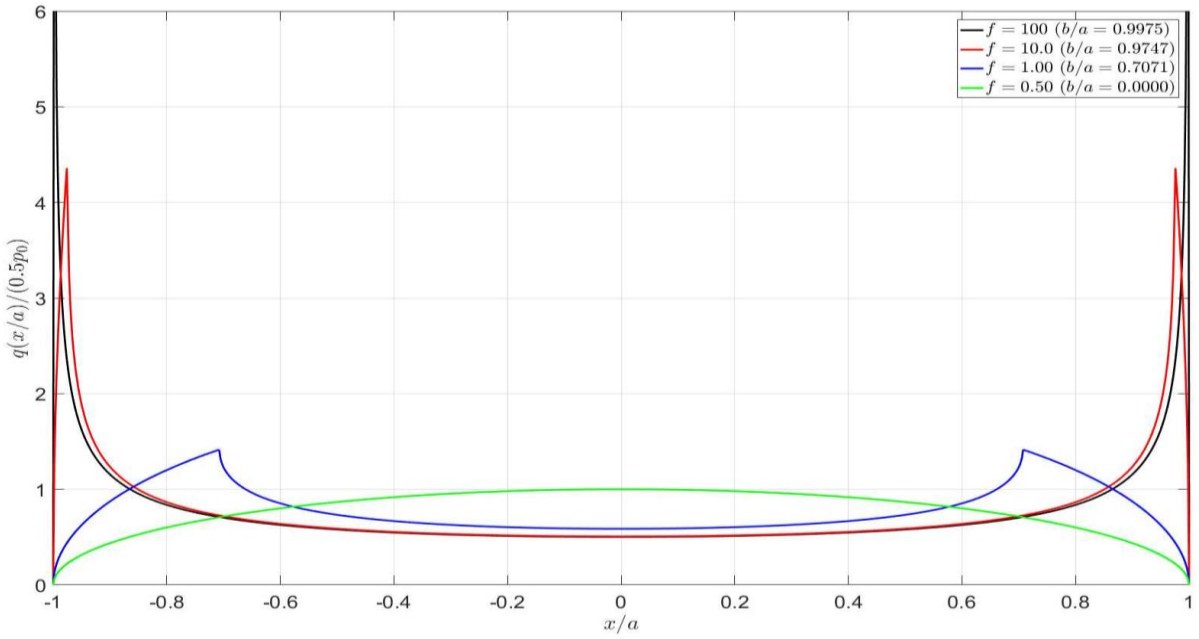


Figure 29 - The size of frictional slip zones at different coefficients of friction

It is obvious that the slip zone is too large to be contained by the plastic envelope. The smallest the plastic zone gets is 1.3 units. So the size of the frictional slip zone need to be smaller than this for the fully stuck condition to be valid.

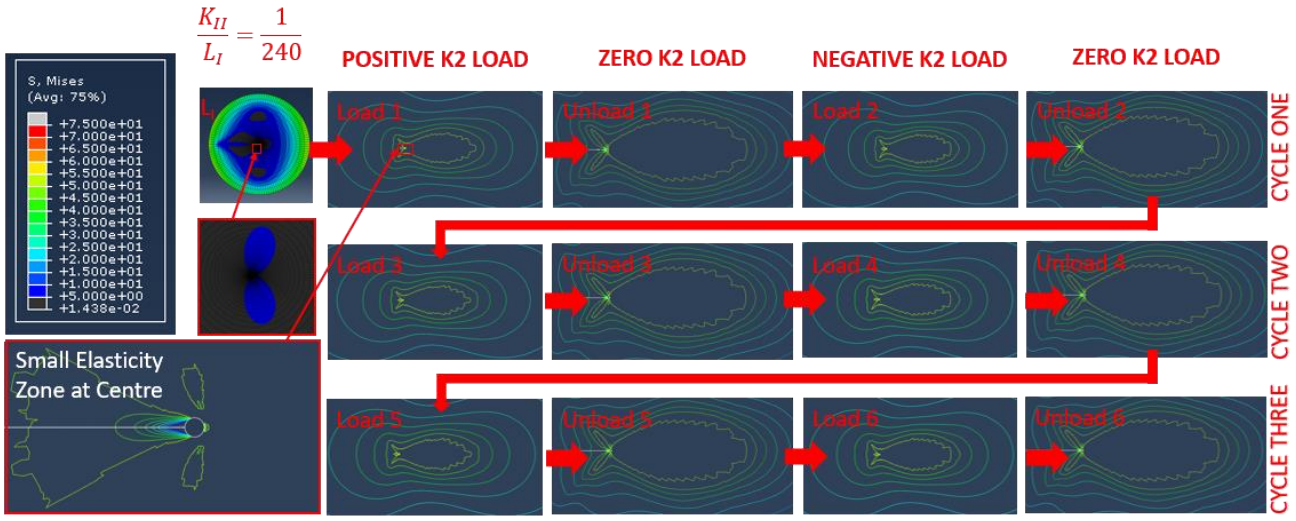
According to Figure 29 the slip zone for a coefficient of friction of 1 (which is, of course, unrealistically high) will give frictional slip up to a value of $(a - 0.7071a) = 0.2929a$. Therefore

$$r_p = \frac{13r_0}{1000} = 0.2929a$$

$$r_0 = 22.5a \tag{148}$$

This is obviously a far larger ratio than the $r_0 = a$ which was used in the analysis done in this thesis. This is due to the fact that the plastic zone was required to be small in relation to the total size of the model in order for small scale yielding conditions to apply. A far larger model would be needed with the area of interest being a small section at the centre such that $a \approx \frac{r_0}{30}$. This would therefore mean that $\frac{K_{II}}{L_I} \leq \frac{1}{240}$ so for a $K_{II} = 5 \times 10^8$ mm$^{1/2}$ MPa it would be required to have $L_I = 12 \times 10^{10}$ mm$^{-1/2}$ MPa.

When we analyse the problem for a much larger L_I value it is still shaken down in the first cycle by the singular field as shown here.



The values of the size of the plastic field are exactly the same as for the lone K_{II} loading and the previous L_I and K_{II} loading. With the obvious exception of the first step where the stresses due to the L_I field are higher and we are just reaching plasticity on the outer edge. In this case we would be

looking just at the central part of the model. This shows that the shakedown still occurs in the same way.

12 *Conclusions and Discussion*

It has been demonstrated that plastic deformation causes a residual stress around the apex of the crack, and of a stuck contact edge. It has been shown also that a 'mode II' residual stress state develops, being of opposite sign to the original loading, and with a concomitant plasticity zone of magnitude approximately ¼ size of the original plasticity zone. This is consistent with the paper 'Cyclic plastic deformation response at fatigue crack tips' (9).

It has been shown that the plasticity zone for the crack tip and incomplete contact interface are not at all similar for simply elastic loading. However, it can be seen that by applying a constant mode I loading to both scenarios and then oscillating a shear load that the two problems become very similar when there is a moderate amount of plastic flow. This is very useful result will allow us to, under certain conditions, to treat a crack tip and an incomplete contact as being, in some sense, equivalent, in terms of the steady state reversing plasticity, and the corresponding 'process zone', and hence their propensity to nucleate cracks.

The other key observation is that in order for a stress field to shake down itself the stress in the second and later loading cycles must be less than the original stress. This is significant as it may cause a large difference in stresses if a load is oscillating from zero to a positive or negative value repeatedly.

13 *Further Work*

One very interesting discovery of this project is that self-shakedown behaviour only occurs when the displacement (and therefore load) in the second and following cycles is less than that in the first cycle. In this project 95% of the displacements is used to ensure this condition is met. It would be very interesting to know if taking the stress to the exact same value will still provide shakedown behaviour. As it is currently unclear if the stress is required to be less than previously loaded or less than or equal to, the theory would indicate less than or equal to would be a sufficient condition. Either of these would not violate the yield surface in any later cycles and so therefore should allow shakedown. In addition it could be investigated if different geometries are used if this behaviour is still seen.

As discussed in Section 11.6 the no slip edge condition is violated with the variables used here. That is to say that the frictional slip zone is larger than the plastic slip zone and therefore cannot be ignored. This model therefore provides the solution for an infinitely large coefficient of friction. More consideration and further models would be required to find when the fully stuck assumption is valid. The problem in this analysis was having a small (relative to the model) plastic zone to allow for small scale yielding which therefore wasn't big enough to encompass the frictional slip in the hertzian contact problem.

We have shown that the crack tip and contact edge geometries are not very similar in the first loading cycle but become very similar after multiple cycles. Therefore in cyclic shear loading the two problems may be treated as one and the same. This will have far reaching implications as all of the fracture mechanics analysis of a crack tip under mode II cyclic loading may now also be applied to an incomplete contact.

As stated earlier in this report the mesh is very fine towards the apex of the crack tip or contact interface but becomes coarser as radius increases. In order to obtain results for the plastic radius with

greater precision the mesh would need to get finer again around the radius of interest in the specific case.

Appendix

Here is a compiled appendices of the stresses and displacements used throughout this project and their origin.

Lawn and Wilshaw (4)

Symmetric Square root singular terms - K_I	$$\begin{pmatrix}\sigma_{rr}\\ \sigma_{\theta\theta}\\ \sigma_{r\theta}\end{pmatrix}_{K_I} = \frac{K_I}{2\pi\sqrt{r}}\begin{bmatrix}\cos\left(\frac{\theta}{2}\right)\left[1+\sin^2\left(\frac{\theta}{2}\right)\right]\\ \cos^3\left(\frac{\theta}{2}\right)\\ \sin\left(\frac{\theta}{2}\right)\cos^2\left(\frac{\theta}{2}\right)\end{bmatrix}$$ $$\begin{pmatrix}u_r\\ u_\theta\end{pmatrix}_{K_I} = \frac{K_I}{2E}\left(\frac{r}{2\pi}\right)^{\frac{1}{2}}\begin{bmatrix}(1+\nu)\left[(2\kappa-1)\cos\left(\frac{\theta}{2}\right)-\cos\left(\frac{3\theta}{2}\right)\right]\\ (1+\nu)\left[-(2\kappa+1)\sin\left(\frac{\theta}{2}\right)+\sin\left(\frac{3\theta}{2}\right)\right]\end{bmatrix}$$
Antisymmetric square root singular terms -K_{II}	$$\begin{pmatrix}\sigma_{rr}\\ \sigma_{\theta\theta}\\ \sigma_{r\theta}\end{pmatrix}_{K_{II}} = \frac{K_{II}}{2\pi\sqrt{r}}\begin{bmatrix}\cos\left(\frac{\theta}{2}\right)\left[1-3\sin^2\left(\frac{\theta}{2}\right)\right]\\ -3\sin\left(\frac{\theta}{2}\right)\cos^2\left(\frac{\theta}{2}\right)\\ \cos\left(\frac{\theta}{2}\right)\left[1-3\sin^2\left(\frac{\theta}{2}\right)\right]\end{bmatrix}$$ $$\begin{pmatrix}u_r\\ u_\theta\end{pmatrix}_{K_{II}} = \frac{K_{II}}{2E}\left(\frac{r}{2\pi}\right)^{\frac{1}{2}}\begin{bmatrix}(1+\nu)\left[-(2\kappa-1)\sin\left(\frac{\theta}{2}\right)+3\sin\left(\frac{3\theta}{2}\right)\right]\\ (1+\nu)\left[-(2\kappa+1)\cos\left(\frac{\theta}{2}\right)+3\cos\left(\frac{3\theta}{2}\right)\right]\end{bmatrix}$$

Calculated

These stresses and displacements have been calculated from first principles with the help of the sources 2 and 3.

Symmetric square root singular terms - K_I	$$\begin{pmatrix}\sigma_{rr}\\ \sigma_{\theta\theta}\\ \sigma_{r\theta}\end{pmatrix}_{K_I} = \frac{K_I}{\sqrt{r}}\begin{bmatrix}\frac{5}{4}\cos\frac{\theta}{2}-\frac{1}{4}\cos\frac{3\theta}{2}\\ \frac{3}{4}\cos\frac{\theta}{2}+\frac{1}{4}\cos\frac{3\theta}{2}\\ \frac{1}{4}\sin\frac{\theta}{2}+\frac{1}{4}\sin\frac{3\theta}{2}\end{bmatrix}$$ $$\begin{pmatrix}u_r\\ u_\theta\end{pmatrix}_{K_I} = \frac{r^{\frac{1}{2}}}{2}\frac{K_I}{2\mu}\begin{bmatrix}-\cos\frac{3\theta}{2}+(2\kappa-1)\cos\left(\frac{\theta}{2}\right)\\ \sin\frac{3\theta}{2}+(2\kappa+1)\sin\left(-\frac{\theta}{2}\right)\end{bmatrix}$$
Antisymmetric square root singular terms -K_{II}	$$\begin{pmatrix}\sigma_{rr}\\ \sigma_{\theta\theta}\\ \sigma_{r\theta}\end{pmatrix}_{K_{II}} = \frac{K_{II}}{\sqrt{r}}\begin{bmatrix}\frac{-5}{4}\sin\frac{\theta}{2}+\frac{3}{4}\sin\frac{3\theta}{2}\\ -\frac{3}{4}\sin\frac{\theta}{2}-\frac{3}{4}\sin\frac{3\theta}{2}\\ \frac{1}{4}\cos\frac{\theta}{2}+\frac{3}{4}\cos\frac{3\theta}{2}\end{bmatrix}$$ $$\begin{pmatrix}u_r\\ u_\theta\end{pmatrix}_{K_{II}} = \frac{r^{\frac{1}{2}}}{2}\frac{K_{II}}{2\mu}\begin{bmatrix}3\sin\frac{3\theta}{2}-(2\kappa-1)\sin\frac{\theta}{2}\\ 3\cos\frac{3\theta}{2}-(2\kappa+1)\cos\frac{\theta}{2}\end{bmatrix}$$
Symmetric square root bounded terms - L_I	$$\begin{pmatrix}\sigma_{rr}\\ \sigma_{\theta\theta}\\ \sigma_{r\theta}\end{pmatrix}_{L_I} = L_I\sqrt{r}\begin{bmatrix}\frac{-3}{4}\cos\frac{\theta}{2}-\frac{1}{4}\cos\frac{5\theta}{2}\\ -\frac{5}{4}\cos\frac{\theta}{2}+\frac{1}{4}\cos\frac{5\theta}{2}\\ -\frac{1}{4}\sin\frac{\theta}{2}+\frac{1}{4}\sin\frac{5\theta}{2}\end{bmatrix}$$ $$\begin{pmatrix}u_r\\ u_\theta\end{pmatrix}_{L_I} = \frac{r^{\frac{3}{2}}L_I}{12\mu}\begin{bmatrix}-\cos\frac{5\theta}{2}+(2\kappa-3)\cos\frac{\theta}{2}\\ 5\sin\frac{5\theta}{2}+(2\kappa+3)\sin\frac{\theta}{2}\end{bmatrix}$$

[1] D.A. Hills. *Corner Asymptotics, Williams' Asymptotic Solution*. Undergraduate Lecture Notes, Department of Engineering Science, University of Oxford (2015).

[2] J.R. Barber. *Elasticity*. Springer, 2nd Edition (2002).

[3] Howatson, Lund and Todd. *Engineering Tables and Data*. Springer, 2nd Edition (1991)

[4] B. R. Lawn and T. R. Wilshaw. *Fracture of Brittle Solids.* Cambridge University Press (1975).

[5] H. Matsunaga, M. Makisaki, D. F. Socie, K. Yanase, M. Endo. *Acceleration of fatigue crack growth due to occasional mode II loading in 7075 aluminium alloy*. Science Direct Journal of Engineering Fracture Mechanics, Volume 123, June 2014, pages 126-136.

[6] A. E. Giannakopoulos, T.C. Lindley and S. Suresh. *Aspects of Equivalence between Contact Mechanics and Fracture Mechanics: Theoretical Connections and a Life-Prediction Methodology for Fretting-Fatigue*. Acta Materialia (1998), 46(9):2955-2968.

[7] M. Jirásek, Z. P. Bazant (2002). *Inelastic Analysis of Structures*. John Wiley and Sons Ltd., New York.

[8] D. Broek. *Elementary Engineering Fracture Mechanics*. Martinus Nijhoff Publishers, 3rd Edition (1984).

[9]Surajit Kumar Paul, S. Tarafder. *Cyclic plastic deformation response at fatigue crack tips.* International Journal of Pressure Vessels and Piping (2012), Volume 101, pages 81-90.

[10] D.A. Hills, R.M.N. Fleury, D. *Dini. Partial slip incomplete contacts under constant normal load and subject to periodic loading*. International Journal of Mechanical Sciences (2016), pages 115-121.